Nonlinear and Linear Modeling of Weatherstrip Seal and Investigation of its Effects in Vehicle Vibrations

by

Emre Dikmen

A Thesis Submitted to the
Graduate School of Engineering
in Partial Fulfillment of the Requirements for
the Degree of

Master of Science
in
Mechanical Engineering

Koc University

September 2006

Koc University

Graduate School of Sciences and Engineering

This is to certify that I have examined this copy of a master's thesis by

Emre Dikmen

and have found that it is complete and satisfactory in all respects,
and that any and all revisions required by the final
examining committee have been made.

Committee Members:

_____

Ipek Basdogan, Ph. D. (Advisor)

_____

Burak Erman, Ph. D.

_____

Murat Sozer, Ph. D.

Date: _____

ABSTRACT

The interior noise level has been an important design criterion lately in automotive industry. Most of the interior noise is generated by the vibrating parts of the vehicle body, mainly the doors. The vibration characteristics of the door panels are affected by the weatherstrip seals. The weatherstrip seals exhibit nonlinear behavior with changing frequency, compression amplitude, temperature and previous load history. Therefore the weatherstrip seals should be modeled accurately in order to predict the dynamic performance of the automobiles under various load conditions. For this purpose, we developed hyperelastic models of the weatherstrip seal using different strain energy functions. In order to estimate the coefficients of the strain energy functions, we used the experimental tension, compression and shear data provided by the manufacturer of the seal. The coefficients were calculated using curve fitting in ANSYS. After the coefficients were calculated, the compression test was simulated in ANSYS using different hyperelastic material models to obtain Compression Load Deflection (CLD) behavior of the weatherstrip seal. Then, compression experiment was conducted using a robotic indenter equipped with force and position sensors. The measured CLD data was then compared with the finite element model (FEM) results and the most suitable hyperelastic model for weatherstrip seal was selected. After the selection of the hyperelastic material model, we obtained the viscoelastic properties of the weatherstrip seal. Viscoelastic properties were obtained using an "Inverse Finite Element Solution" technique which required the hyperelastic material properties as an initial guess. Stress relaxation tests were performed using the robotic indenter to determine the viscoelastic properties. The required constants were calculated using an optimization algorithm in ANSYS utilizing the experimental relaxation data as the reference point.

Independent from the previous studies, we built a Single Degree of Freedom (SDOF) system to determine equivalent stiffness and damping coefficients for the weatherstrip seal. The set-up includes a mass and weatherstrip seal underneath to simulate a spring and a dashpot system. Experimental modal analysis of the system was performed and equivalent stiffness and damping for the weatherstrip seal were determined.

Finally, we conducted experimental and numerical modal analysis of the vehicle door with and without the weatherstrip seal. Experimental modal analysis was performed with two different configurations to determine the effect of the seal and the boundary conditions on the vibration characteristics of the vehicle. Numerical modal analysis was performed by constructing the finite element model of the system and simulating the same conditions in the computer environment. Equivalent stiffness values calculated from the SDOF system experiment were used in the FEM. The experimental and model predicted results were compared and the effect of the seal on the vehicle dynamics was determined.

ÖZET

Otomotiv endüstrisi için taşıt içi gürültü seviyesi önemli bir tasarım kriteri olmaya başlamıştır. Taşıt içi gürültünün önemli bir kısmı taşıt gövdesindeki, özellikle de kapılardaki titreşimden kaynaklanmaktadır. Araç kapılarının titreşimi, kapı fitilinden etkilenmektedir. Kapı fitili frekansla, sıcaklıkla, sıkışma miktarıyla değişen lineer olmayan davranış göstermektedir. Bu nedenle taşıtların dinamik performansını tahmin etmek için kapı fitillerinin doğru bir şekilde modellenmesi yapılmalıdır. Bu amaçla farklı hiperelastik malzeme modelleriyle kapı fitilinin sıkışmasının sonlu elemanlar yöntemi kullanılarak ANSYS yazılımı vasıtasıyla benzetimi yapılmıştır. Bu malzeme modellerinin tanımlanması için gerekli katsayıların tespitinde üretici firmadan alınan deney sonuçları kullanılmıştır. Bu deney sonuçları ANSYS yazılımına aktarılmış ve bu sayede gerekli malzeme modeli katsayıları tespit edilmiştir. Bu katsayılar elde edildikten sonra farklı hiperelastik malzeme modelleri kullanılarak sıkıştırma deneyinin benzetimi ANSYS yazılımında yapılmıştır. Daha sonra sıkıştırma deneyi hassas bir cihazla yapılmış, farklı modeller kullanılarak yapılan benzetim sonuçlarıyla karşılaştırılarak kapı fitilinin modellenmesi için en uygun hiperelastik malzeme modeli tespit edilmiştir. Uygun hiperelastik malzeme modeli tespit edildikten sonra evrik sonlu elemanlar yöntemi geliştirilerek viskoelastik malzeme modelleri de önceki modele ilave edilmiştir.

Bu çalışmalardan bağımsız olarak tek serbestlik dereceli bir deney düzeneği kurulmuş ve bu deney düzeneği kullanılarak kapı fitili için eşdeğer yay sabiti bulunmuştur.

Son olarak deneysel ve sonlu elemanlar yöntemi kullanılarak araç kapısının modal analizi yapılmıştır. Deneysel modal analizde kapı fitilinin ve sınır şartların etkisini tespit etmek maksadıyla iki ayrı deney düzeneği kullanılmıştır. Bu düzeneklerin ilkinde araç kapısı elastik iplerle asılmıştır. İkincisinde ise araç havalı yaylarla kaldırılmış, kapı gerçek çalışma koşullarındaki sınır şartları ile test edilmiştir. Aynı şartlarla kapının modal analizi

sonlu elemanlar yöntemiyle kapı fitili yerine tek serbestlik dereceli sistemden elde edilen yay sabitleri kullanılarak yapılmıştır. Bu yay sabitleri kullanılarak yapılan sonlu elemanlar analizi sonuçları ile deney sonuçlarının birbirlerine oldukça yakın olduğu gözlemlenmiştir.

ACKNOWLEDGEMENTS

I would like to express my sincere gratitude and appreciation to my advisor, Assist. Prof. Dr. İpek Başdoğan for her expert guidance, suggestions and constructive criticisms at all phases of this study. I am grateful to Assist. Prof. Dr. İpek Başdoğan also for her generous and continuous support in other phases of my life.

I would like to thank to Dr. Mert Doğanlı, İlker Yılmaz of Ford Otosan A.S and Dr. Tuncay Yüksel of Standart Profil A.S. for their kindness, sharing their knowledge, their valuable suggestions during my research and sparing their time whenever I need help.

I also want to thank to Mert Sedef for his cooperation to perform compression experiments.

I am very grateful to my family and special friends; Satayef Kassabbashi, Emrah Ahi and Murat Ötkür for their support and motivation during my research.

TABLE OF CONTENTS

LIST OF TABLES

LIST OF FIGURES

NOMENCLATURE

A	Accelerance
C	damping matrix
DVs	design variables
E	effective elastic modulus
E(t)	elastic relaxation function
J	volume ratio
K	stiffness matrix
L	final length
M	mass matrix
N	number of the Maxwell elements
R	receptance
SVs	state variables
W	strain-energy function
c	viscous damping coefficient
d	material incompressibility parameter
k	stiffness
m	mass
r	frequency ratio
Δu	elongation
x	displacement
α	material constant for Ogden strain energy function
ε	strain
$\Delta\varepsilon$	infinitesimal strain increment
λ	stretch ratio
η	structural damping coefficient

μ	initial shear modulus
ω	frequency
$\Delta\omega$	frequency bandwith
σ	stress
$\Delta\sigma$	infinitesimal stress increment
τ	relaxation time
ξ	viscous damping ratio
C_{10}, C_{01}	coefficients of Mooney-Rivlin strain-energy function
F_j^{EXP}	experimental force value of j^{th} data point
F_j^{FEM}	force value of j^{th} data point obtained from FEM simulation
I_1, I_2, I_3	principle strain invariants
J_m	limiting value of I_1-3
L_0	initial length
W_b	volumetric part of the strain-energy function
W_d	deviatoric part of the strain-energy function
$\dot{x}$	velocity
$\ddot{x}$	acceleration
ε_D	strain in a dashpot
ε_E	engineering strain
ε_S	strain in a spring
$\lambda_1, \lambda_2, \lambda_3$	principal stretch ratios
λ_L	limiting network stretch
σ_D	stress in a dashpot
σ_S	stress in a spring
ω_n	natural frequency

Chapter 1

INTRODUCTION

Dynamic and acoustic behavior of vehicles is a crucial issue for the automotive industry with the increasing demand for better passenger comfort. Vibration may lead to passenger discomfort and interior noise. Interior noise can be classified as structure borne or airborne. Airborne noise is a result of the wind, sound radiation from the tires, engine and exhaust system of a vehicle. Previous studies state that the main reason of the low frequency structure borne noise is the vibrating panels enclosing the vehicle. Engine generates high amount of excitation in a wide range of frequency and vibration is transferred from the engine mounts to all around the structures passing through the rigidly connected parts. At low frequencies, excitation coming from the engine causes the panels such as; roof, floor, body side, dashboard, and doors to vibrate at their resonant frequencies. Consequently, vibrating panels cause a change in the sound pressure level inside and undesirable booming noise results in the passenger compartment.

The vehicle door is one of the noise sources contributing to the overall panel vibrations. Boundary conditions and the weatherstrip seals affect the dynamics of the doors considerably. Automotive weatherstrip seals are mainly used to prevent water and dust entrance to the passenger compartment in all weather conditions and accommodate for the manufacturing variations. The seal strip runs all around the perimeter of the door. When the door is closed, it remains in contact with the opening panel through the hinges at the front side, the lock mechanism at the rear side and through the seal strip all around the door

perimeter. They exhibit nonlinear behavior with changing frequency, compression amplitude, temperature and previous load history and induce some residual stiffness and viscoelastic contribution to the door support conditions. Therefore their effect on door vibrations can be significant and should be studied to understand the overall vehicle dynamics.

In this study, we present an approach for modeling the weatherstrip seals using hyperelastic and viscoelastic material models available in ANSYS. The modeling approach was supported by experimental studies conducted in our laboratories. An equivalent linear spring and dashpot system was also built to represent the weatherstrip seal in FEM simulations to decrease the computational cost.

The following chapter provides necessary background and literature review related to the modeling and simulation of the weatherstrip seal using hyperelastic and viscoelastic material models. The relation of the panel vibrations and vehicle acoustics are also reviewed. Chapter 3 briefly reviews the theoretical background of hyperelasticity, linear viscoelasticity, mechanical vibrations and modal analysis. Details of the nonlinear modeling of the weatherstrip seal are given in Chapter 4. In particular, compression experiments, determination of the suitable hyperelastic model and details of the inverse finite element method to viscoelastic and hyperelastic properties of the seal are presented. Details of a single degree of freedom system to determine the equivalent linear spring and dashpot model for the weatherstrip seal are given in Chapter 5. Chapter 6 presents the modal properties of the automobile weatherstrip seal determined from the experiments made with two different setups. Results of the finite element simulation using the spring coefficients determined from the single degree of freedom system are also given in Chapter 6. Finally, the thesis is concluded with the discussion and conclusion section.

Chapter 2

LITERATURE REVIEW

2.1 Overview

Rubber can withstand large deformations (up to 600-700% strains) without permanent deformation and have higher damping characteristic compared to other materials. Due to its superior properties, rubber is widely used as a flexible structural joint between stiff components in automotive and other engineering applications. Vibration isolators in engine mounts, dampers in helicopter rotors, seismic isolators of large structures, exhaust hanger and automotive door weatherstrip seals are typical examples of such applications. However, mechanical properties (e.g. hardness, stiffness, strength, stress-strain relation) of rubber are not well known. This is due to the fact that these properties may vary with the amount of deformation, previous load history, temperature, frequency and amplitude of the motion in the presence of mechanical vibrations. Besides, hysteresis and rate effects are significant in determining the characteristics of the rubber like materials. Therefore, many researchers performed experiments in order to identify mechanical properties of structures made of rubber.

At low frequencies, excitation coming from the engine causes the panels such as roof, floor, body side, dashboard, and doors to vibrate at their resonant frequencies. Consequently, vibrating panels cause a change in the sound pressure level inside and undesirable booming noise results in the passenger compartment. The vehicle door is one

of the noise sources contributing to the overall panel vibrations. The weatherstrip seal results in stiffness and viscoelastic contribution to the door support conditions therefore it affects the dynamics of the car door considerably. As a result, accurate representation of the seals is crucial in the simulation models.

2.2. Material Characterization and Modeling of Structural Parts Made of Rubber

Recently, commercial finite element analysis programs are widely used to make accurate simulations of engineering problems decreasing the cost of the design, number of experiments and design period. Therefore accurate modeling and material characterization of the rubber parts are necessary. However rubber properties are difficult to obtain since it exhibits nonlinear behavior changing with time, frequency of vibration, compression amount and temperature. There are some studies about material characterization and modeling of rubber in the literature.

Some researchers performed experimental work in order to characterize material properties of rubber and model the rubber structures as a spring dashpot system. Pan et al. [1] presented a simple experimental method to evaluate the frequency dependent rubber mount stiffness and damping characteristics by utilizing the measured complex frequency response function from impact test and by least-squares polynomial curve fitting the data obtained from the test. They constructed a single degree of freedom (SDOF) system which consists of a mass block and rubber underneath. They proposed a method to model the rubber mount as a spring-damper system. The proposed method was validated by comparing its results with those obtained using mechanical shaker excitations and those of conventional direct stiffness method using blocked transfer frequency response functions. Kren and Vriend [2] used dynamic indentation test method in order to determine viscoelastic properties of rubber. Experimental and theoretical curves for velocity, force

and penetration in the indentation process were compared for rubbers with different hardness. Besides, a semi-empirical relationship between the Shore hardness and the rigidity *c* was derived. Fenander [3] measured the vertical stiffness and damping of studded rubber railpads, both in a complete track and in a test rig, as functions of frequency under different static preloads. Also, for more compact polymer-based railpads, track measurements were performed. The stiffness of the studded railpads was found to increase strongly with preload, but only weakly with frequency. The loss factor of the studded railpads was found to be nearly independent of preload and to increase slightly only with frequency. He proposed a fractional derivative model for the dynamic behaviour of the railpad.

As the finite element simulations become widely applicable, modeling of the rubber made structures become an important issue in obtaining reliable simulation results. Wagner et al. [4] analyzed automotive weatherstrip seal for compression load deflection (CLD) behavior, contact pressure distribution and aspiration (loss of contact between the weatherstrip seal and the facing sheet metal surface) due to a pressure differential across the seal by using nonlinear finite element analysis. They modeled weatherstrip seal via Blatz-Ko and Mooney Rivlin hyperelastic material models and compared resultant CLD behavior with Linear Elastic Model. Stenti et al. [5] performed nonlinear static and dynamic analysis by using commercial finite element code MSC Marc with a simplified car door weatherstrip seal model. CLD behavior was obtained via static analysis and the effect of deformation amount of seal to the vibration modes of the door was analyzed using dynamic analysis. Lu et al. [6] performed nonlinear finite element analysis (FEA) and experiments for a rubber mount under large deformation to obtain its static characteristics. Experimental results agreed well with the FEA results. The static strain–stress analysis of the rubber part showed that the von Mises stress could be adopted as a stress measure for the rubber material. Moreover, the modeling methods for the large deformation rubber

mount were investigated with numerical tests of elastic characteristics. In another study, a test structure which simulated the door and the body was constructed [7]. Natural frequencies of the structure were obtained by the experiments performed, in the cases of with and without seals lying between the two frames. It was verified that the seal caused a frequency shift in the test structure. Simulations of the both cases were performed by finite element analysis and an equivalent spring coefficient was determined for the weatherstrip seal. In another study; Valenta and Molnar [8] made the comparison of two material models, Mooney-Rivlin and Neo-Hooke by using Marc Mentat FEM software for silicone rubber which is a non-linear incompressible elastic material with large deformability. Gur and Morman [9] applied nonlinear finite element analysis to determine the conditions conducive to seal system aspiration. Using this analysis procedure, they determined the effect on aspiration of such parameters as initial seal height, seal shape, seal thickness, seal constitutive model, friction and seal compression due to door closing. Then, this analysis tool had been applied to production vehicles in order to determine the aspiration characteristic of glass-run seal systems.

2.3. Automotive Panel Vibrations

One of the common problems in automotive engineering is the noise resulted from the interior body panels. It is the result of the transverse vibrations of the panels caused by the preceding structure-borne noise transmission from the excitation source. In automotive engineering, modal analysis is a widely used methodology to determine the sound quality and vibration performances of the vehicles. Modal behavior of a vehicle is examined in order to determine characteristic properties of the structure such as natural frequency.

In order to improve characteristics including vehicle interior noise, several different studies are done such as; different schemes of beads to decouple structural and acoustic

resonance modes, numerical optimizations including geometry of body joints, increasing the lowest eigenfrequency of a sedans floor panel, roof and dashboard minimizing the structural transfer function [10],[11],[12],[13].

In his study, Lim [10] divided the body structure encompassing the passenger space into a number of panels having similar geometrical and transverse vibration response characteristics. Then, he measured the noise transfer functions from each part of the panels and distributed the overall noise generated to each panel with respect to these measured partitions. Finally, the contributions of all panels were examined and it was concluded that at some frequency range side panels were the major contributor to the high sound pressure level inside the passenger compartment.

Marburg et al. [11], optimized floor panel concerning only the noise resulting from the oscillation of this panel. Mode shapes, the natural frequencies of these shapes and the noise level due to these vibrations were calculated. Then panel was stiffened by inserting beads on it and the difference in the modes' frequency and noise level was determined. Finally optimum bead geometries were defined.

Kim et al. [12] proposed a practical method for noise reduction and applied this method to a medium size test car. The proposed method was based upon the structural-acoustic response model, in which the interior pressure was explicitly described in terms of the modal parameters and structural-acoustic modal coupling coefficients of the car body and compartment system. They used only some of the modes and modal coupling coefficients which had large contributions for identifying the cause of the noise peak and reducing interior noise level. This study was performed using software (ACSTAP) which was developed through this research.

Marburg et al. worked in another study [13] to develop a reliable simulation model which runs in a reasonable time. They tuned simulation model with respect to modes found in the experimental modal analysis. It was shown that the relatively large decreases of noise

transfer that were predicted by simulation and optimization were also found in the experiment. This verification, however, was impossible if the simulation model cannot predict the major effects that are responsible for noise. In the application used in this study, these effects were well included for frequencies up to 50 Hz. For frequencies above 50 Hz, the simulation model was likely to be too stiff, which is assumed to be due to an insufficiently detailed modeling at the edges and welding joints. An optimization process included positioning and length of additional beams.

Chapter 3

THEORETICAL BACKGROUND

3.1 Introduction to Hyperelasticity

Hyperelasticity refers to the materials which can experience large elastic strain that is recoverable. Elastomers such as rubber and many other polymer materials fall in this category. The constitutive behavior of hyperelastic materials are usually derived from the strain energy potentials. Also, hyperelastic materials generally have very small compressibility. This is often referred to as "incompressibility". The hyperelastic material models assume that materials response is isothermal. This assumption allows that the strain energy potentials are expressed in terms of strain invariants or principal stretch ratios. Stretch ratio is basically defined for uniaxial tension as [14]:

$$\lambda = \frac{L}{L_0} = \frac{L_0 + \Delta u}{L_0} = 1 + \varepsilon_E \qquad (3.1)$$

where L is the final length, L_0 is the initial length, Δu is the elongation and ε_E is the engineering strain. There are three principal stretch ratios $\lambda_1, \lambda_2, \lambda_3$ which can be used to define the strain energy potential. The principal stretch ratios λ_1 and λ_2 characterize in-plane deformation. On the other hand, λ_3 defines the out-of-plane deformation.

Strain invariants are measures of strain which are independent of the coordinate system used to measure the strains. Three strain invariants are usually used to define strain energy function [14].

$$I_1 = \lambda_1^2 + \lambda_2^2 + \lambda_3^2 \tag{3.2}$$

$$I_2 = \lambda_1^2\lambda_2^2 + \lambda_2^2\lambda_3^2 + \lambda_3^2\lambda_1^2 \tag{3.3}$$

$$I_3 = \lambda_1^2\lambda_2^2\lambda_3^2 \tag{3.4}$$

Constitutive behavior of hyperelastic materials are generally derived from the strain energy potentials. The strain energy potentials which are generally denoted as W are functions of principal stretch ratios or strain invariants. Volumetric (with subscript b) and deviatoric (with subscript d and bar) terms of the strain energy function for incompressible materials are shown below in order to represent the volumetric term as a function of J [14].

$$W = W_d(\bar{I}_1, \bar{I}_2) + W_b(J) \tag{3.5}$$

$$W = W_d(\bar{\lambda}_1, \bar{\lambda}_2, \bar{\lambda}_3) + W_b(J) \tag{3.6}$$

where J is the ratio of the final volume to the initial volume and $\bar{\lambda}_p$ and $\bar{I}_p$ terms are (for p=1, 2, and 3):

$$\bar{\lambda}_p = J^{-1/3}\lambda_p \tag{3.7}$$

$$\bar{I}_p = J^{-2/3}I_p \tag{3.8}$$

Rubber exhibits hyperelastic and viscoelastic behavior. We used a commercial finite element software; ANSYS in order to model the weatherstrip seal and obtain the compression load deflection (CLD) behavior. However there are many hyperelastic material models available in ANSYS. Therefore, the first step was to determine the suitable hyperelastic model to be used for the subsequent analysis. In order to determine the suitable hyperelastic model, we performed compression simulations and compared the results with the experiments done at 0.05 mm/s compression speed using a robotic indenter.

The coefficients required for the hyperelastic models are calculated automatically via linear or nonlinear regression curve fitting algorithms available in ANSYS. We used the following tests to calculate these coefficients: Simple Tension, Simple Compression and Simple Shear. The required coefficients and curve fitting algorithms for the strain energy potential functions (hyperelastic models) that we used in our study are shown in Table 3.1.

A brief description of the hyperelastic material models used in our analysis are as follows:

Table 3.1**:** Material Constants and Curve fitting Algorithms [14]

Hyperelastic Model	Coefficients found by curve fitting	Curve fitting Algorithm
Mooney Rivlin	c_{10}, c_{01}, d	Linear Regression
Arruda-Boyce	$\mu\ , \lambda_L, d$	Nonlinear Regression
Ogden	μ, α, d	Nonlinear Regression
Blatz-Ko	μ	Nonlinear Regression
Gent	μ, J_m, d	Nonlinear Regression

3.1.1 Mooney-Rivlin Model

Mooney-Rivlin Model is very simple in formulation therefore it is widely used in hyperelastic applications such as rubber and tissue simulations. There are two, three, five, and nine-term Mooney Rivlin models available in ANSYS. The two-term Mooney-Rivlin model may be valid up to 90-100% tensile strains; however it is not usually efficient to simulate the stiffening behavior present at large strains. Compression behavior may also not be characterized well with only two-term Mooney Rivlin model [14].

The strain energy potential for two term Mooney-Rivlin model is:

$$W = c_{10}\left(\overline{I_1} - 3\right) + c_{01}\left(\overline{I_2} - 3\right) + \frac{1}{d}(J-1)^2 \qquad (3.9)$$

where c_{10}, c_{01} are material constants for Mooney-Rivlin model and d is material incompressibility parameter. Material constants c_{10} and c_{01} are calculated using the curve fitting algorithm in ANSYS with the simple tension, simple compression and simple shear

test data for EPDM sponge rubber provided by the manufacturer of the weatherstrip seal. The incompressibility parameter d is disregarded due to the unavailability of volumetric test data. Therefore, volumetric term involving the volume ratio J, is ignored.

3.1.2 Arruda-Boyce Model

The Arruda-Boyce form is a statistical mechanics-based model. This means that the form was developed as a statistical treatment of non-Gaussian chains emanating from the center of the element to its corners. This model is generally limited to 300% strain [14].

The strain energy potential for Arruda- Boyce model is:

$$W = \mu \sum_{i=1}^{5} \frac{C_i}{\lambda_L^{2i-2}} \left(\bar{I}_1^{\,i} - 3^i \right) + \frac{1}{d} \left(\frac{J^2 - 1}{2} - \ln J \right) \qquad (3.10)$$

where the constants C_i are:

$$C_1 = \frac{1}{2},\ C_2 = \frac{1}{20},\ C_3 = \frac{11}{1050},\ C_4 = \frac{19}{7050},\ C_5 = \frac{519}{673750}$$

Also material constants μ , λ_L are determined by using curve fitting algorithm of ANSYS with simple tension, simple compression and simple shear test data. As it is explained in the previous section, incompressibility parameter d can not be calculated due to unavailability of the volumetric test data, eliminating the volumetric component of the strain energy density function.

3.1.3 Ogden Model

The Ogden form is directly based on the principal stretch ratios rather than the strain invariants:

$$W = \sum_{i=1}^{N} \frac{\mu_i}{\alpha_i} \left(\bar{\lambda}_1^{\alpha_i} + \bar{\lambda}_2^{\alpha_i} + \bar{\lambda}_3^{\alpha_i} - 3 \right) + \sum_{i=1}^{N} \frac{1}{d_i} (J-1)^{2i} \qquad (3.11)$$

Ogden model is based on principal stretch ratios directly; therefore it may be more accurate and may provide better data fitting. However, it may also be more computationally expensive. In general, Ogden form may be applicable for strains up to 700% [14].

In this study, first order Ogden model is used and required material coefficients μ, α are obtained by ANSYS using simple tension, simple compression and simple shear test data. Volumetric component (the term including volume ratio J) is not taken into account as in the previous models leading to incompressible material behavior assumption.

3.1.4 Blatz-Ko Model

Blatz-Ko model is used for the modeling of compressible foam-type rubbers. The strain energy potential function is:

$$W = \frac{\mu}{2} \left(\frac{I_2}{I_3} + 2\sqrt{I_3} - 5 \right) \qquad (3.12)$$

where μ is a material constant and determined by using ANSYS curve fitting algorithm.

3.1.5 Gent Model

The strain energy potential function for Gent model is:

$$W = \frac{\mu J_m}{2} \ln\left(1 - \frac{I_1 - 3}{J_m}\right)^{-1} + \frac{1}{d}\left(\frac{J^2 - 1}{2} - \ln J\right) \qquad (3.13)$$

The material constants μ, J_m are determined by using curve fitting algorithm available in ANSYS using the simple tension, simple compression and simple shear test data.

3.2 Introduction to Linear Viscoelasticity

Rubber exhibits hyperelastic and viscoelastic behavior. The second step to model the weatherstrip seal using ANSYS was to characterize the viscoelastic material properties of the weatherstrip seal. A viscoelastic material is characterized by both elastic and viscous behavior. For a purely elastic material, all the energy stored in the sample during loading is returned when the load is removed. As a result, loading and response curves for elastic materials move completely in phase (Figure 3.1.a). A purely viscous material does not return the energy stored during loading (Figure 3.1.b). All the energy is lost as "pure damping" once the load is removed. These materials have only damping component and no stiffness component. Viscoelasticity is concerned with materials which exhibit both elastic and viscous behavior. Some of the energy stored in a viscoelastic system is recovered upon removal of the load, and the remainder is dissipated in the form of heat. Therefore, a phase difference occurs between loading and response curves (Figure 3.1.c) [15].

In viscoelastic materials, an instantaneous elastic response is observed upon loading, and then a slow and continuous change in the response at a decreasing rate is obtained.

When the load is removed, a continuously changing response follows an initial elastic recovery as illustrated in Figure 3.2.

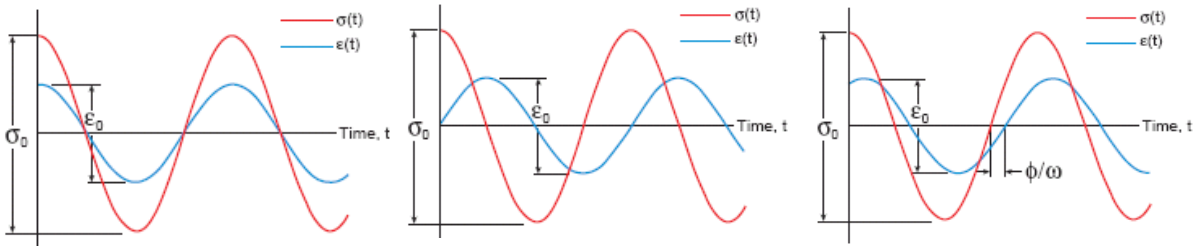

a) b) c)

Figure 3.1: Cyclic loading and response curves for various materials: a) Elastic material, b) Viscous material, and c) Viscoelastic material [15]

Such viscoelastic materials are significantly influenced by the rate of straining or stressing; i.e., for example, the longer the time to reach the final value of stress at a constant rate of stressing, the larger is the corresponding strain [16]. Since time plays an important role in the behavior of viscoelastic materials, they are also called time-dependent materials. This time-dependency is explained by the phenomena of creep under constant stress and stress relaxation under constant strain as given in Figure 3.2. We performed stress relaxation tests and used this test data in inverse finite element solution to characterize viscoelastic material properties.

Time dependency of stress relaxation function E can be more conveniently given by spring and dashpot models. In these models, the stress carried by the spring is proportional to the strain and is given by Hooke's law (Equation 3.14). The stress carried in the dashpot is proportional to the strain rate and is given by Newton's law of viscosity (Equation 3.15). Viscoelastic materials then can be modeled as combination of springs and dashpots in series or parallel.

$$\sigma = E\varepsilon \tag{3.14}$$

$$\sigma = \eta \frac{d\varepsilon}{dt} \tag{3.15}$$

The Maxwell model given in Figure 3.3 is a series connection of a spring and a dashpot. In this model ε_S and σ_S denote the strain and stress in the spring alone and ε_D and σ_D denote those in the dashpot alone [17]. Total strain in the Maxwell model is given by

$$\varepsilon = \varepsilon_S + \varepsilon_D \tag{3.16}$$

and if we differentiate both sides, we end up with

$$\frac{d\varepsilon}{dt} = \frac{1}{E}\frac{d\sigma_S}{dt} + \frac{\sigma_D}{\eta} \tag{3.17}$$

Since $\sigma = \sigma_S = \sigma_D$ then

$$\frac{d\sigma}{dt} + \frac{\sigma}{\tau} = E\frac{d\varepsilon}{dt} \tag{3.18}$$

where

$$\tau = \frac{\eta}{E} \tag{3.19}$$

is the so called relaxation time. Using $\sigma(0) = \varepsilon(0) = 0$, this ODE can be solved to give

$$\sigma(t) = \int_0^t E \exp(-\frac{t-s}{\tau}) \frac{\partial \varepsilon(s)}{\partial s} ds \qquad (3.20)$$

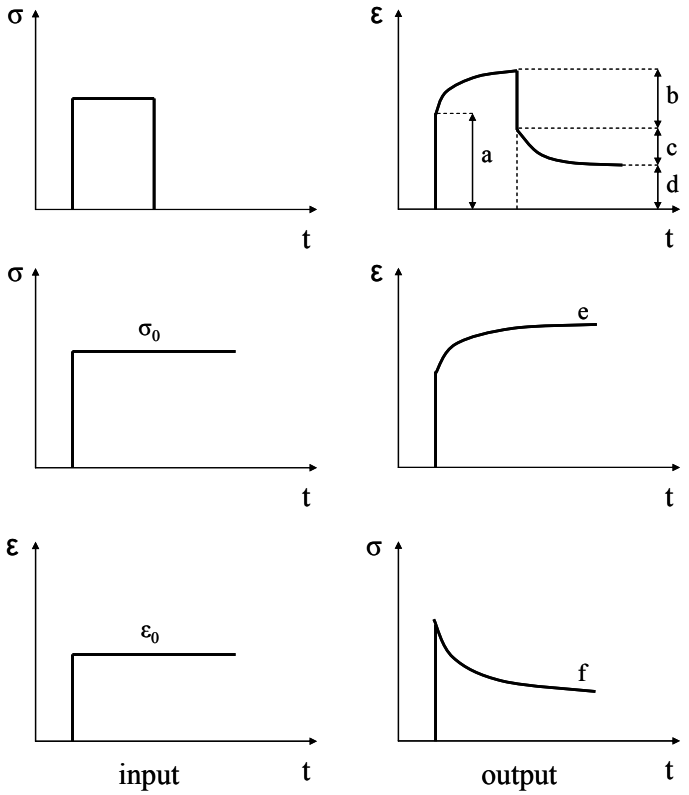

Figure 3.2: Viscoelastic phenomena: a. Instantaneous elastic response, b. Instantaneous elastic recovery, c. Delayed recovery, d. Permanent set, e. Creep under constant stress, f. Stress relaxation under constant strain [16].

This derivation can be applied to Generalized Maxwell Solid element given in Figure 3.4 to end up with a Prony Series expression for relaxation function. The Generalized Maxwell model and Prony series representation of the stress relaxation functions are used in ANSYS to model viscoelastic behavior.

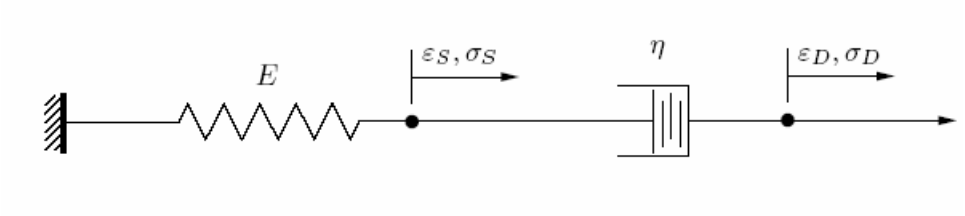

Figure 3.3: The Maxwell model [17]

$$E(t) = E_{\infty} + \sum_{j=1}^{N} E_j \exp\left(-\frac{t}{\tau_j}\right) \tag{3.21}$$

where, N is the number of the Maxwell elements (Figure 3.3) in generalized form, E_j is the independent stiffness parameter and τ_j is the relaxation time given in Equation 3.19.

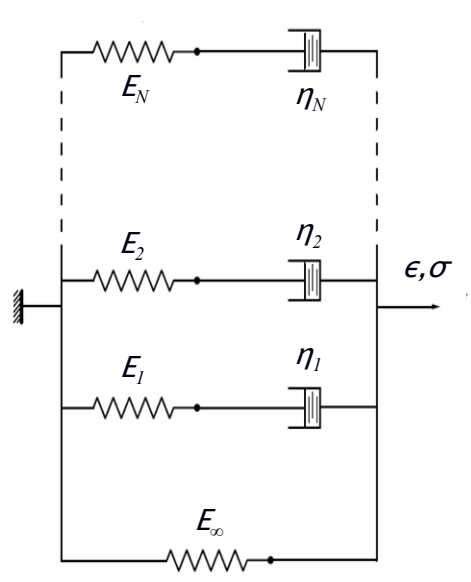

Figure 3.4: The generalized Maxwell solid, which is a combination of springs and dashpots with independent stiffness and viscosity parameters [17]

3.3 Introduction to Mechanical Vibrations and Modal Analysis

Modal Analysis is the process of determining the inherent dynamic characteristics of a system in forms of natural frequencies, damping factors and mode shapes, and using them to formulate a mathematical model for its dynamic behavior. The formulated mathematical model is referred as the modal model of the system and the information for the characteristics is known as its modal data. Modal Analysis has become a major technology for determining, improving and optimizing dynamic characteristics of engineering structures. Modal Analysis is based upon the fact that the vibration response of a linear time-invariant dynamic system can be expressed as the linear combination of a set of simple motions called the natural modes of vibration. The natural modes of vibration are inherent to a dynamic system and are determined completely by its physical properties (mass, stiffness, damping) and their spatial distributions [18].

In this study, we performed experimental modal analysis of a single degree of freedom setup consisting of a mass and weatherstrip seals underneath. Then we used this data to model the weatherstrip seal as a spring and dashpot system which may be used in subsequent finite element simulations. We also performed the experimental modal analysis of the car door in different configurations to evaluate the effects of weatherstrip seal and boundary conditions. Afterwards we used all these data in ME'Scope VES to determine mode shapes and modal frequencies of the structure. ME'Scope VES matches a parametric form of FRF to experimental data and obtains mode shapes, modal frequencies, modal damping as a result. ME'Scope VES uses a non-proportional damping model explained below in detail:

3.3.1 Modal Analysis of a damped MDOF system-Non-proportional Damping Model

If the damping distribution of the system of n degree of freedoms (dof) with viscous damping is denoted as a matrix [C], the matrix equation of motion of the system is given by [18]:

$$[M]\{\ddot{x}\} + [C]\{\dot{x}\} + [K]\{x\} = 0 \tag{3.22}$$

When the viscous damping of n dof system is non-proportional, the solution of equation (3.22) is in the form:

$$\{x(t)\} = \{X\}e^{st} \tag{3.23}$$

Here, s is the Laplace operator and {X} a complex vector for displacement amplitudes. Then equation (3.22) becomes:

$$(s^2[M] + s[C] + [K])\{X\} = \{0\} \tag{3.24}$$

The solution to this problem is possible with state space representation approach. This approach generates a new displacement vector defined as:

$$y = \begin{Bmatrix} x \\ \dot{x} \end{Bmatrix} \tag{3.25}$$

Then, Equation (3.22) is transferred into:

$$\begin{bmatrix} C & M \\ M & 0 \end{bmatrix} \begin{Bmatrix} \dot{y} \end{Bmatrix} + \begin{bmatrix} K & 0 \\ 0 & -M \end{bmatrix} \begin{Bmatrix} y \end{Bmatrix} = \{0\} \tag{3.26}$$

or $$[A]\begin{Bmatrix} \dot{y} \end{Bmatrix} + [B]\{y\} = \{0\} \tag{3.27}$$

Equation (3.27) is a normal eigenvalue problem and its solution consists of 2n complex eigenvalues λ_r and 2n corresponding complex eigenvectors $\{\theta\}_r$ satisfying the following equation.

$$(\lambda_r[A] + [B])\{\theta\}_r = \{0\} \qquad (r=1,2,\ldots..2n) \tag{3.28}$$

The equation of motion of an MDOF system with non-proportional structural damping is given by equation (3.29).

$$[M]\begin{Bmatrix} \ddot{x} \end{Bmatrix} + [K]\{x\} + j[H]\{x\} = 0 \tag{3.29}$$

The solution can be assumed as

$$\{x(t)\} = \{X\}e^{j\lambda t} \tag{3.30}$$

Where λ is the complex frequency accommodating both oscillation and free decay of the vibration and $\{X\}$ is a complex vector for displacement amplitudes. This form of solution, once substituted into equation (3.29), leads to a complex eigenvalue problem:

$$\left([K]_c - \lambda^2[M]\right)\{X\} = \{0\} \tag{3.31}$$

The solution to the equation (3.31) will yield a diagonal eigenvalue matrix $[\lambda_r]$ and an eigenvector matrix $[\psi]$. Where $\lambda_r^2 = \omega_r^2(1 + j\eta_r)$

Chapter 4

NONLINEAR MODELING OF THE WEATHERSTRIP SEAL

4.1 Introduction

Rubber exhibits nonlinear, elastic and time-dependent behavior which is characterized by hyperelastic and viscoelastic models. Finite Element Modeling (FEM) of rubber for static and dynamic analysis is now possible with hyperelastic and viscoelastic material models included in the commercial FEM packages. However, simulation of rubber exhibits some difficulties due to material nonlinearity and modeling of contact and boundary conditions. Another difficulty is choosing appropriate material model among many options which are described with different strain energy functions. There are some studies in the literature [4],[5] performed previously to obtain CLD behavior of the weatherstrip seals, however these studies do not compare FEM predictions with experimental results and they use simplified hyperelastic models [5].

This section summarizes the procedure that we followed to determine the most suitable hyperelastic model to represent the weatherstrip seal and inverse finite element solution to obtain viscoelastic and hyperelastic material model. Finite Element Model of the seal was built in ANSYS using different hyperelastic models. Coefficients of the different strain energy functions were calculated using both linear and nonlinear square curve fitting in ANSYS. The fitted data includes the tension, shear and compression test results obtained from the manufacturer of the seal.

After the coefficients were calculated, the compression test was simulated in ANSYS using different hyperelastic material models. The CLD behavior of the seal was obtained by increasing the load incrementally and recording the displacement at each time step. The details of the hyperelastic models used in this study are given in Section 3.1. This chapter also includes the inverse FEM approach that is used to determine the hyperelastic and viscoelastic properties of the weatherstrip seal.

4.2 Hyperelastic Material Modeling

ANSYS requires one or more of the following tests to calculate coefficients of material models: Simple Tension, Simple Compression, Biaxial Tension, Planar Shear, Simple Shear and Volumetric Test. The test data is collected as engineering stress and strain. A typical engineering stress-strain curve for a rubber sample under cyclic loading is shown in Figure 4.1. Hysteresis (behavior in loading and unloading is different) and stress softening effects (such as Mullins effect) are also present for rubber. Therefore a stabilized curve is required for curve fitting in ANSYS. One should have data for the three modes of deformation in order to fully characterize the material. The test data should also cover the complete strain range of interest.

We used the curve fitting algorithm in ANSYS with simple tension, simple compression and simple shear test data provided by the manufacturer of the weatherstrip seal to calculate the necessary coefficients of hyperelastic models.

Simple tension experiments are very widely used for rubber like materials. There are some experimental requirements for such tests. The most significant requirement is that in order to achieve a state of pure tensile strain, the specimen should be much longer in the direction of stretching than in the width and thickness dimensions. The objective is to perform an experiment where there is no lateral constraint to specimen thinning [19].

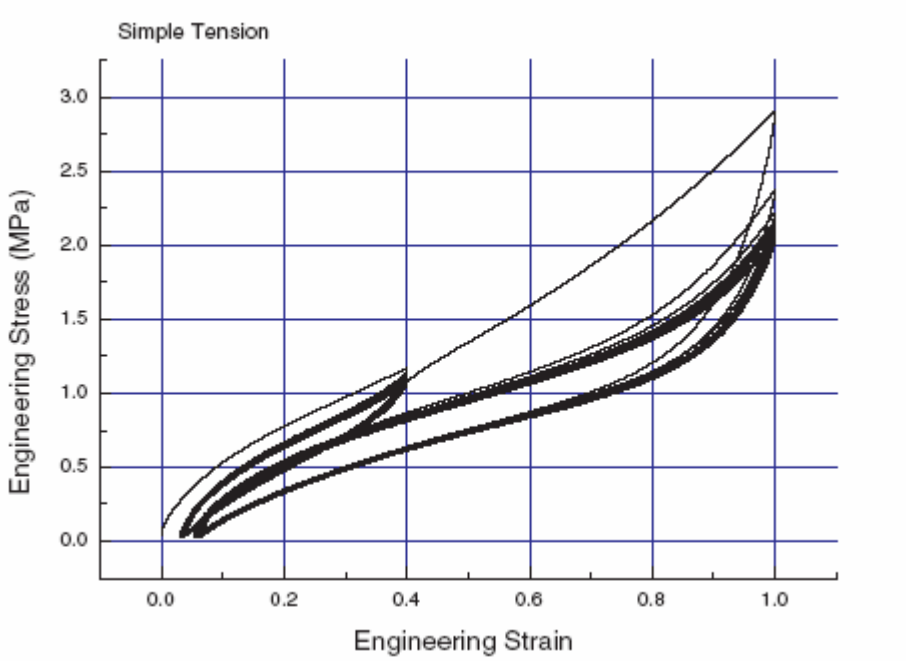

Figure 4.1: A typical engineering stress-strain curve for a rubber sample under cyclic load

Specimen clamps create an indeterminate state of stress and strain in the region surrounding the clamp in the process of gripping. Therefore, the specimen straining must be measured on the specimen, but away from the clamp, where a pure tension strain state is occurring. A non-contacting strain measuring device such as a video extensometer or laser extensometer is required to achieve this (see Figure 4.2) [19].

The simple shear experiment appears to be very similar to tensile test. However, because the material is nearly incompressible, a state of pure shear exists in the specimen at a 45 degree angle to the stretching direction. The most significant aspect of the specimen is that it should be much shorter in the direction of stretching than the width. The objective is to create an experiment where the specimen is perfectly constrained in the lateral direction such that all specimen thinning occurs in the thickness direction.

A non-contacting strain measuring device must be used to measure strain away from the clamp edges where the pure strain state is occurring (Figure 4.3) [19].

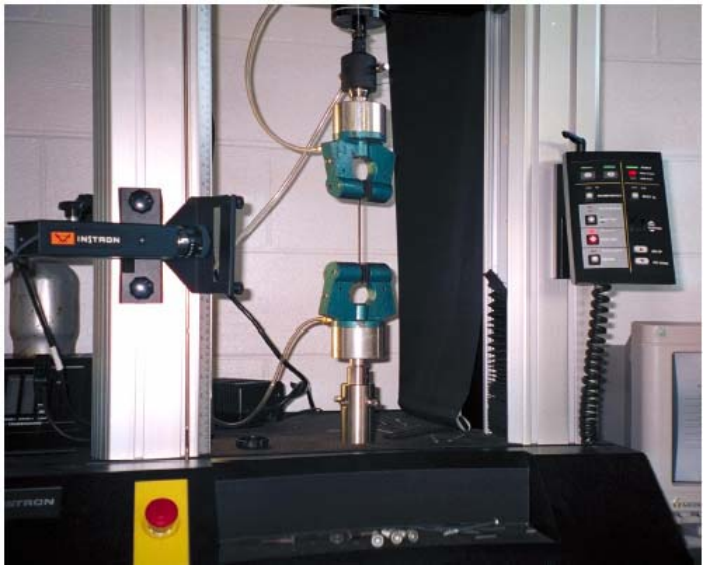

Figure 4.2: A tension experiment using a video extensometer [19]

The simple compression experiment is also used widely for rubber like materials. When testing for analysis, pure states of strain are desired and this is especially difficult to achieve experimentally in compression. Because there is friction between the test specimen and the instrument platens, the specimen is not completely free to expand laterally during compression. Even very small of friction coefficient levels such as 0.1 between the specimen and the platen can cause substantial shearing strains that alter the stress response to straining (Figure 4.4) [19].

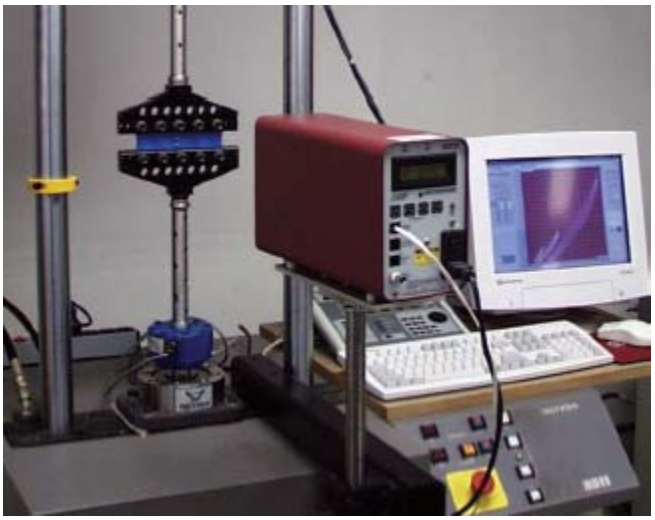

Figure 4.3: A shear experiment using a laser extensometer [19]

Figure 4.4: A lubricated compression specimen showing lateral constraining from friction [19]

Parameter characterization of hyperelastic models in ANSYS relies on a least square curve fitting algorithm. Multiple types of test are required to cover different deformation and to ensure the accuracy [14].

In this study; the coefficients required for the hyperelastic models defined in section 3.1 are found using simple compression, simple tension and simple shear test data provided by the manufacturer of the weatherstrip seal. The results of these three tests are illustrated by the Figures 4.5-4.7.

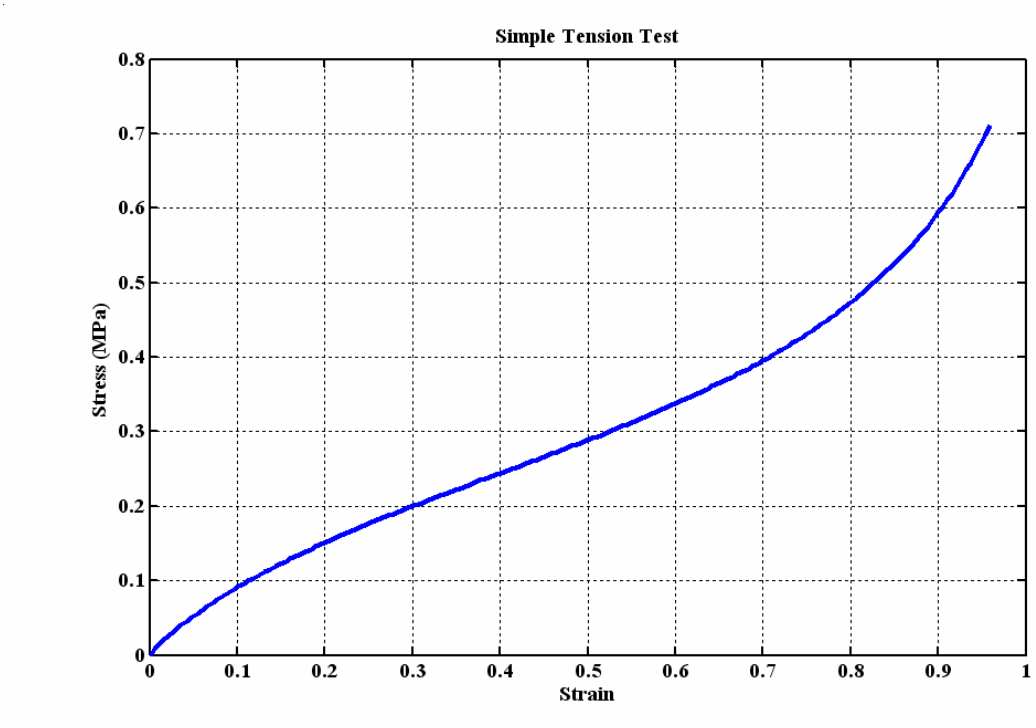

Figure 4.5: Simple tension test results for weatherstrip seal sample

The procedure to find the material model constants by using the test explained above is as follows:

1. Inputting the experimental data
2. Specifying hyperelastic material model

3. Fitting the experimental data
4. Updating the material data to ANSYS database

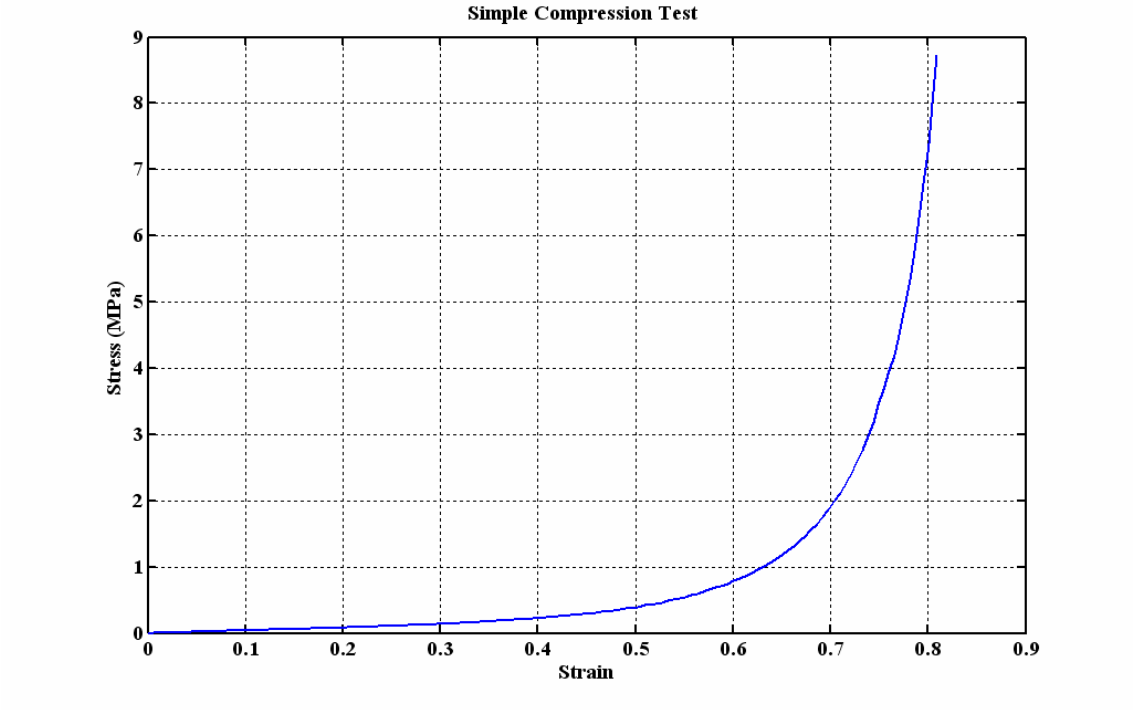

Figure 4.6: Simple compression test results for weatherstrip seal sample

4.2.1 Geometric Modeling and Assumptions

The original geometry was imported to ANSYS in IGES (Initial Graphics Exchange Specification) format. Plane Strain assumption was applicable since there was no deformation in the depth direction. Therefore, analysis was made with two dimensional models decreasing the computational time drastically. Plane 182 elements were used in the analysis due to its hyperelasticity, viscoelasticity, large deflection, and large strain capabilities. Figure 4.8 shows the meshed model of the weatherstrip seal. Compressing

plate was simulated as a rigid line. Displacement of 14 mm was applied to the plate incrementally and force data was obtained at each increment.

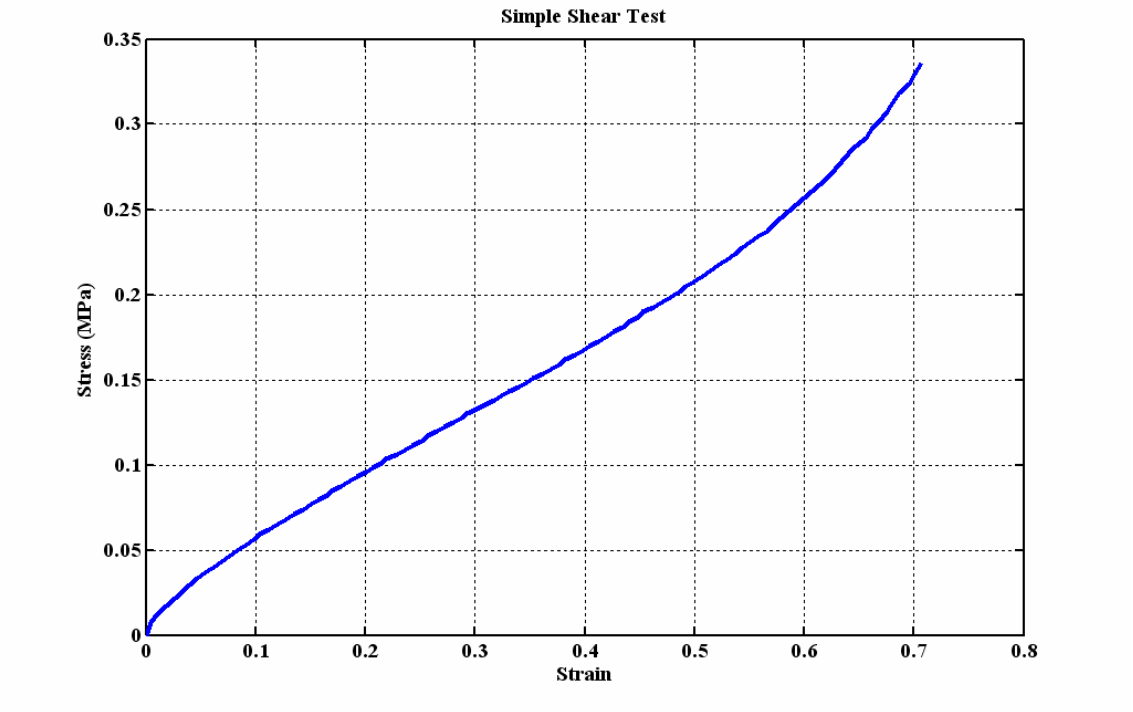

Figure 4.7: Simple shear test results for weatherstrip seal sample

4.2.2 Comparison of FE results and Compression Experiments

Compression experiments were conducted using a robotic indenter equipped with force and position sensors. A graphical user interface (GUI) and a PID controller were used to move the indenter from an initial position to a desired position in 3D space in discrete time steps while compensating for positional errors. Compression speed and displacement were entered in GUI to move the indenter to the desired displacement value with constant speed. A force-torque transducer (Nano 17 from ATI Industrial Automation) was used for the

purpose of measuring force response. The Nano 17 has a force range of ±70 N in the normal direction, ±50 N in other principal directions and has a resolution of 1/1280 N along each of the three orthogonal axes when attached to a 16-bit A/D converter.

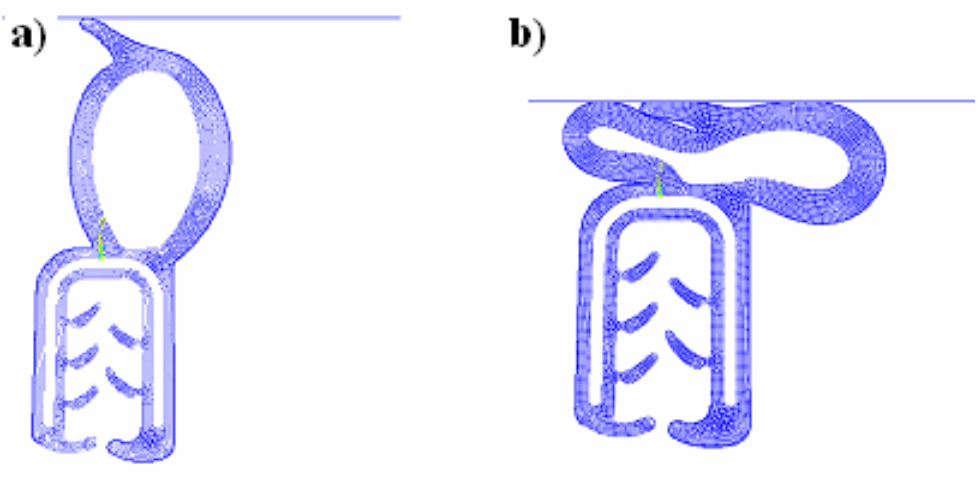

Figure 4.8: Finite element model of the weatherstrip seal
a) before compression and b) after compression

Data acquisition unit includes a 16-bit analog input card NI PCI-6034E (National Instruments) with a maximum sampling rate of 200 kS/s [20]. The experimental set-up for the compression test is shown in Figure 4.9.

Compression speed was chosen as 0.05 mm/s in order to minimize the dynamic effects providing data similar to the quasistatic compression case in ANSYS. Experiments were repeated a couple of times and the results were averaged in order to minimize the experimental errors. For FEM simulations, Simple Tension, Simple Compression and Simple Shear Test results obtained from the manufacturer were used to find the coefficients required for Ogden, Arruda-Boyce, Gent, Mooney-Rivlin and Blatz-Ko models.

The coefficients listed in Table 3.1 were calculated using the curve fitting algorithms of ANSYS for each hyperelastic material model.

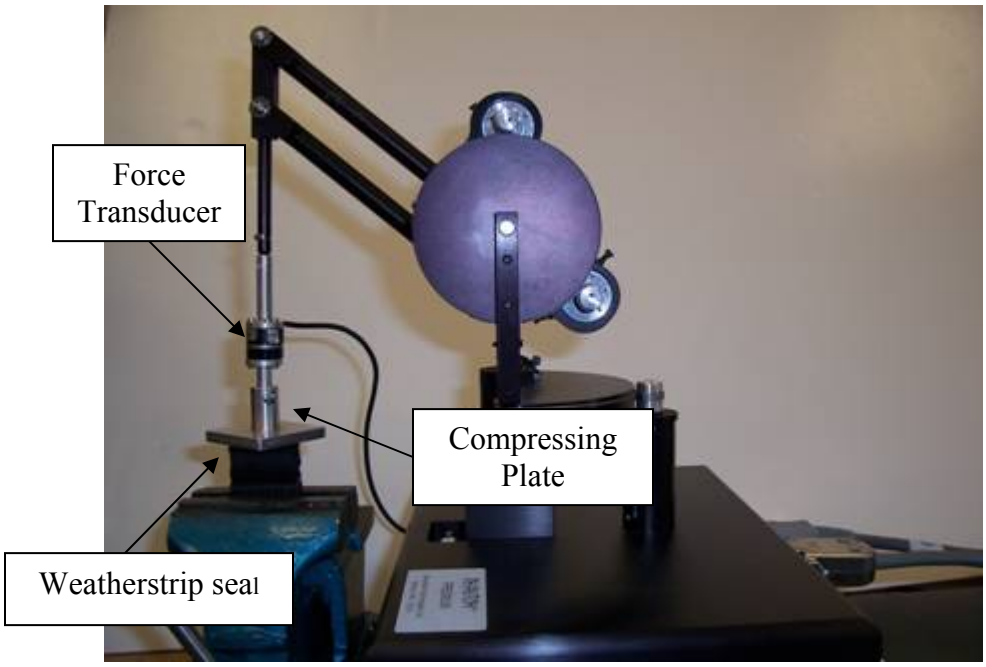

Figure 4.9: Experimental setup for compression tests

Figure 4.10 shows the FEM results and compression experiment at 0.05 mm/s. Ogden and Arruda-Boyce models resulted in similar force values with the experiments but stiffening of rubber at large displacements (above 11 mm) were not observed in the FEM results. The differences between the experimental and model predicted results can be explained by the inaccurate modeling assumptions in ANSYS. The volumetric test data was unavailable from the manufacturer and it is believed that this may affect the accuracy of the curve fitting which was initially used to calculate the coefficients of the hyperelastic models. Also, the FEM and the real specimen can exhibit some geometrical differences due to the nature of the manufacturing process of the weatherstrip seal.

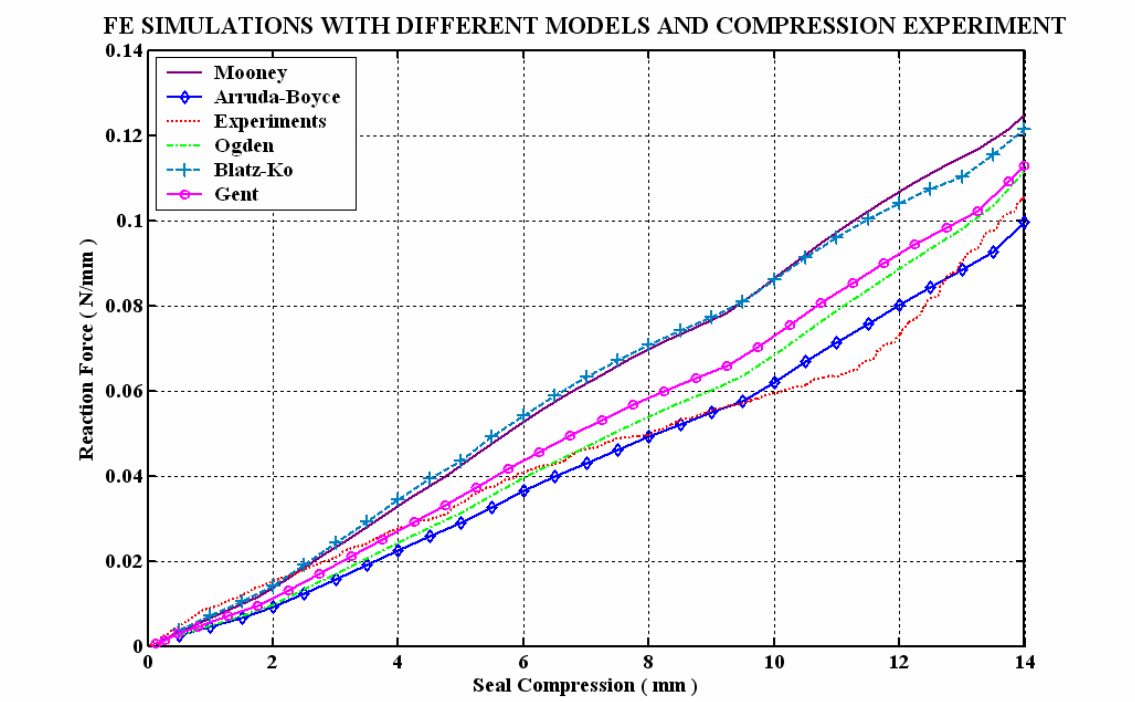

Figure 4.10: Comparison of FEM results with the experiments

Generally there is only uniaxial tension test data available for the curve fitting process; therefore the accuracy of using only uniaxial test data to determine coefficients of material models is investigated. Ogden and Arruda-Boyce Models are shown to be efficient to simulate the compression case in Figure 4.10. Consequently these models are used in simulations made by using only uniaxial test data. Simulation results with uniaxial test data and experiments are shown in Figure 4.11. It is observed that uniaxial test data by itself is insufficient for the compression simulations of weatherstrip seal.

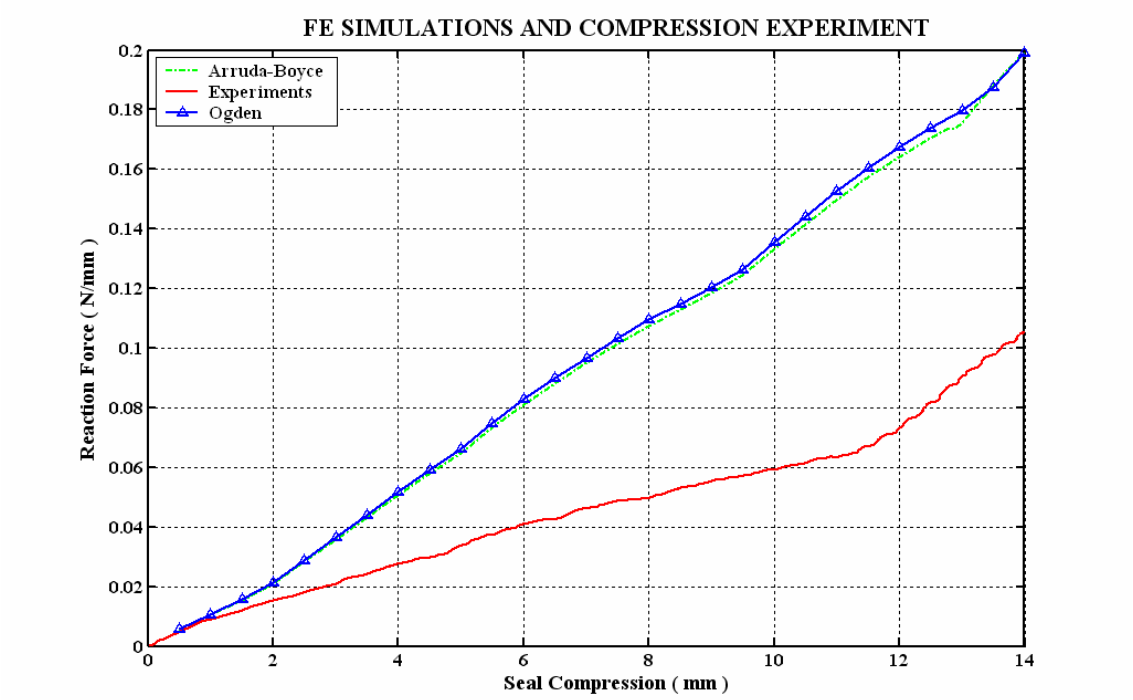

Figure 4.11: Comparison of compression experiment with the simulations using only uniaxial test

A very significant observation made during deformation of rubber is the "Mullins effect" [21]. The Mullins effect is associated mainly with a significant reduction in the stress at a given level of strain at successive loading and unloading conditions. Mullins effect recovers with time being on the order of hours or days [22]. The experiments explained above are conducted in succession and Mullins effect is not observed. ANSYS results reveal that only a small portion of the weatherstrip seal experiences large strains, therefore significant stress softening effect do not occur (See Figure 4.12).

Another important issue is the coefficient of friction in the FEM. Coefficient of friction between the weatherstrip seal and contacting surface is uncertain.

FEM simulations are made with friction coefficients 0.4 and 1 (See Figure 4.13). As it can be seen from the figure, CLD behaviors for different friction coefficients are very similar. It is concluded that friction coefficient does not play an important role in reaction forces since they act in the direction of the normal of the contacting surfaces.

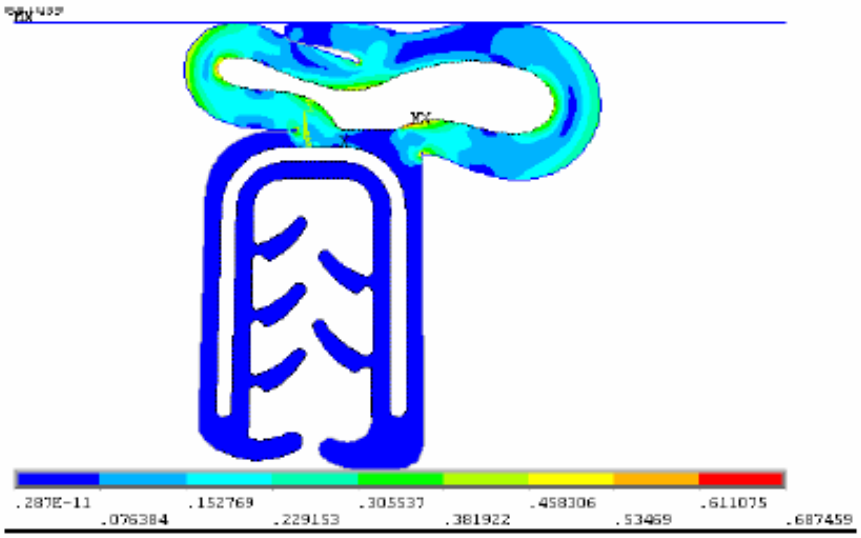

Figure 4.12: Equivalent Von Mises strain distribution

In conclusion, we used FEM to determine CLD behavior of automobile weatherstrip seals with different hyperelastic models and the model predictions are compared with the experimental results. Ogden and Arruda-Boyce models using simple tension, compression and shear test data are found to be the most suitable strain energy functions for modeling the weatherstrip seals.

It is observed that using only simple tension test data to determine required coefficients of the hyperelastic model is insufficient to obtain accurate results for CLD behavior of the weatherstrip seal. The "Mullins effect" and "friction coefficient effect" are also investigated and they are found to be insignificant for this type of application.

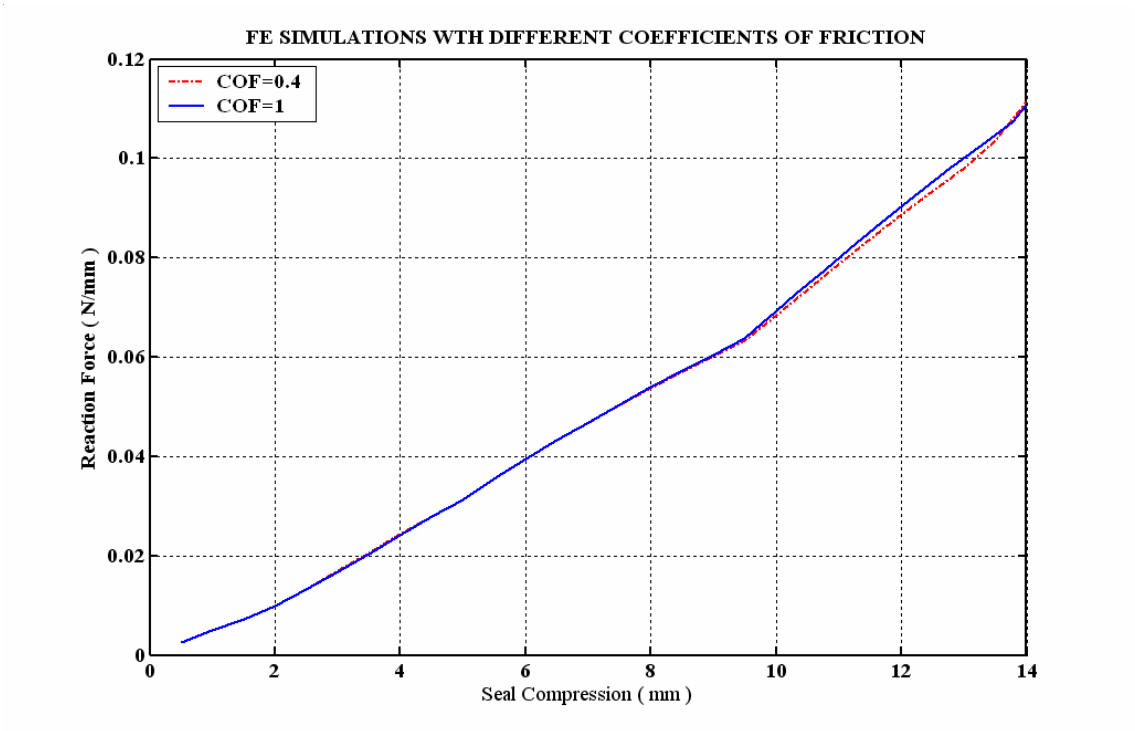

Figure 4.13: Comparison of FEM results with different friction coefficients

4.3 Inverse finite element solution

As explained in section 3.2, time dependent behavior is characterized by viscoelastic material models. The hyperelastic materials do not involve time-dependent properties; therefore viscoelastic material properties should be added to the nonlinear model if rubber exhibits viscoelastic behavior.

Viscoelasticity is a rate-dependent behavior where the material properties may be both time- and temperature-dependent. Viscoelastic response can be thought of as being comprised of both an elastic and viscous part [14].

In order to observe viscoelastic behavior of the weatherstrip seal, stress relaxation experiments with indentation depths of 4, 8, 10 and 14 mm were performed. The robotic indenter reached to the predefined indentation depth in one second and it was held there for 40 seconds to characterize the viscoelastic response of the weatherstrip seal. The step input assumption is used in the analysis. Stress relaxation experiments for a 30 mm long weatherstrip seal with indentation depths of 4 and 8 mm (corresponding to compression speeds of 4 and 8 mm/s) are shown in Figure 4.14 and 4.15.

It is observed from the stress relaxation tests that weatherstrip seal exhibits viscoelastic behavior. Viscoelastic materials are significantly influenced by the rate of loading. As the strain rate decreases, viscoelastic behavior disappears. To capture the whole stress relaxation behavior, high loading rates are required. In order to model viscoelastic behavior of the weatherstrip seal, we used ANSYS to simulate the Stress Relaxation Test in the computer environment. ANSYS uses a Prony series representation of the stress relaxation functions to model viscoelasticity [14]. The deviatoric stress expression is formulated in ANSYS for large strain viscoelasticity as:

$$s = \int_0^t \left[\alpha_\infty + \sum_{j=1}^{2} \alpha_j \exp\left(-\frac{t-\tau}{\tau_j} \right) \right] \left(2 \frac{d}{d\tau} \frac{dW}{dC} \right) d\tau \qquad (4.1)$$

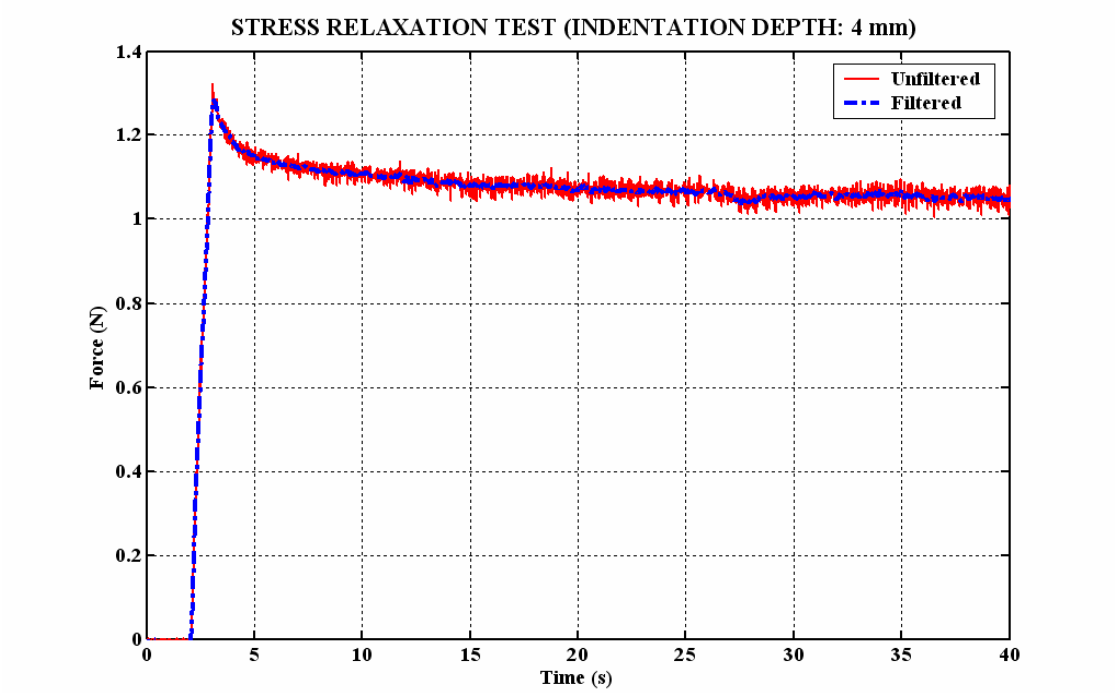

Figure 4.14: Stress Relaxation Experiment with 4 mm indentation depth

Where α_1, τ_1, α_2, τ_2 are Prony series coefficients, $\boldsymbol{G_0}$ is the short term shear modulus, $\boldsymbol{W}$ is a strain energy function of a hyperelastic model and C is the right Cauchy-Green deformation tensor. These coefficients must be estimated through the use of an optimization algorithm (see Figure 4.16) while performing the Stress Relaxation Test in ANSYS. Optimization routine minimizes an objective error function that is defined between the actual (experimental) and the simulated forces. In order to perform an optimization analysis in ANSYS, three set of variables must be defined. First set consists of independent quantities called *design variables* (*DVs*) to be determined by the optimization algorithm. Second set contains *state variables* (*SVs*) constraining the model and finally, a dependent variable (*objective function*) to be minimized must be determined. The *sub-problem* optimization algorithm uses approximations (curve fitting) to determine the optimum values of *DVs* [14].

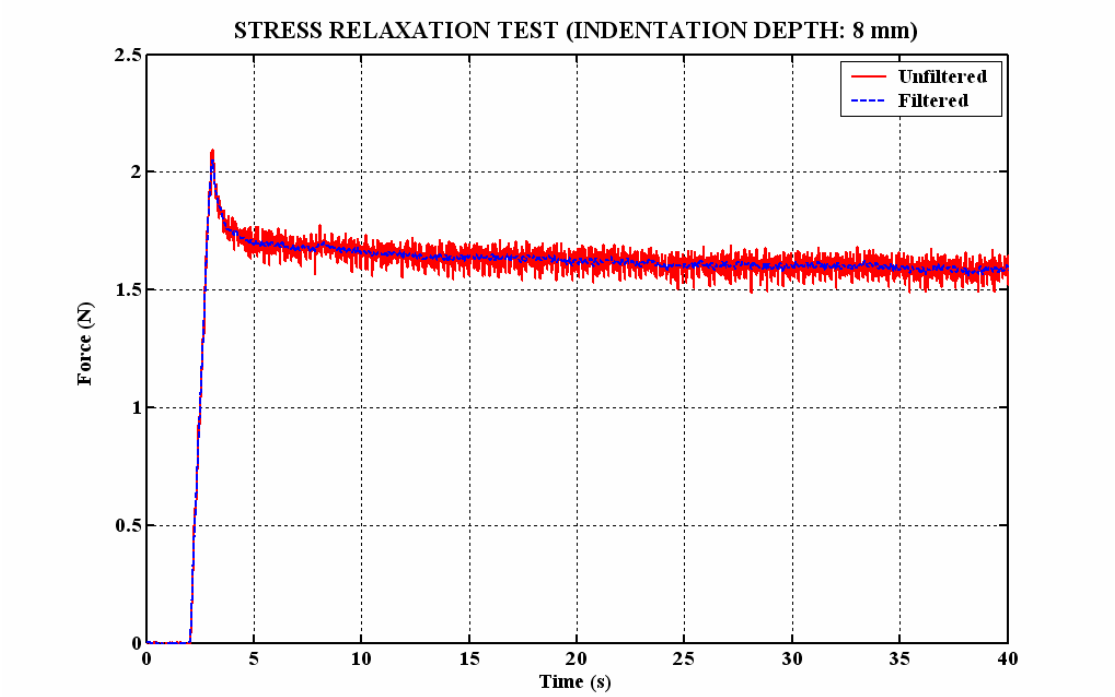

Figure 4.15: Stress Relaxation Experiment with 8 mm indentation depth

In order to extract the material properties of the weatherstrip seal, an inverse finite element solution was developed. The characterization of material properties based on experimental data was considered as the "inverse problem". Figure 4.16 illustrates the inverse finite element procedure. The finite element model defined previously in section 4.2.1 was used in the optimization analysis. Stress relaxation simulation was performed by using the hyperelastic and viscoelastic models. Previously determined coefficients from Section 4.2 were used as initial guesses for hyperelastic models. The initial guesses for viscoelastic models were selected arbitrarily. Hyperelastic material behavior was modeled using Arruda-Boyce strain-energy function given in Equation 3.10 and viscoelasticity was modeled using 2-term Prony series.

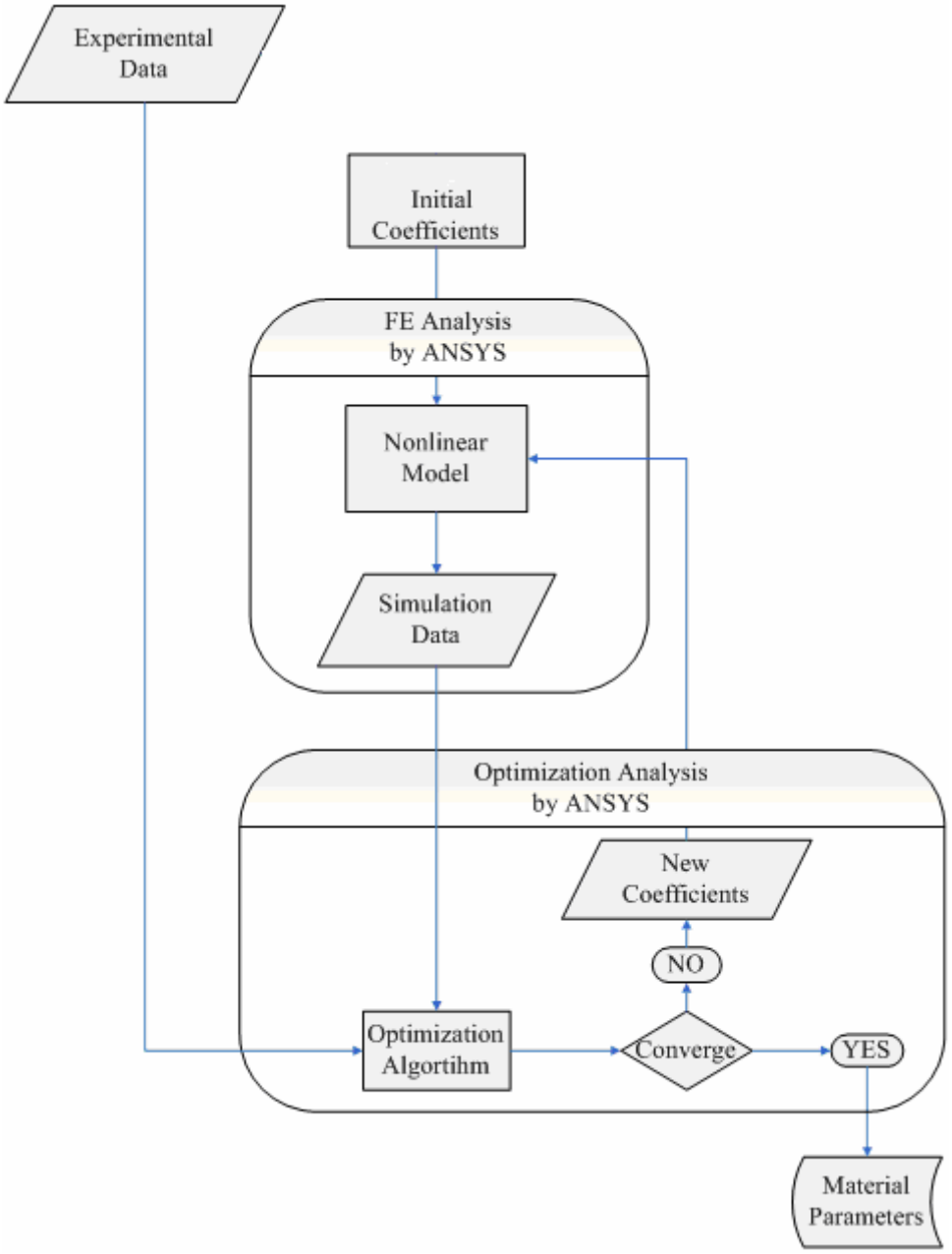

Figure 4.16: Inverse finite element procedure

To calculate the hyperelastic and viscoelastic parameters of the weatherstrip seal, μ , λ_L α_1, τ_1, α_2 and τ_2 were assigned as *DVs*. 8 data points, (i.e. force samples representing the relaxation behavior), were chosen from the experimental force relaxation data and then compared with the force values (i.e. *SVs*) obtained from the finite element solution. The optimization algorithm minimizes the *objective function* defined as:

$$\text{Error} = \sum_{j=1}^{8} \left(F_j^{EXP} - F_j^{FEM} \right)^2 \qquad (4.2)$$

where F_j^{EXP} is the experimental force value of j^{th} data point and F_j^{FEM} is the force value obtained from the FEM simulation at the corresponding time. If the error is greater than the specified value of 0.01, simulation is done again modifying the design variables. This loop continues till the error becomes less than the specified value. Consequently; the hyperelastic model coefficients, μ , λ_L and viscoelastic model coefficients α_1, τ_1, α_2, τ_2 were determined via the inverse finite element solution.

4.3.1 Inverse FE Solution Results

Experimental force relaxation curve for 8 mm indentation (strain rate is 8 mm/s) and the FE simulation with the material properties obtained from inverse FE solution are illustrated in the Figure 4.17. Stress relaxation test data was used in the inverse FE solution to determine the material viscoelastic and hyperelastic model coefficients. Then, these coefficients were used in stress relaxation simulations which exhibits good correlation with the experiments.

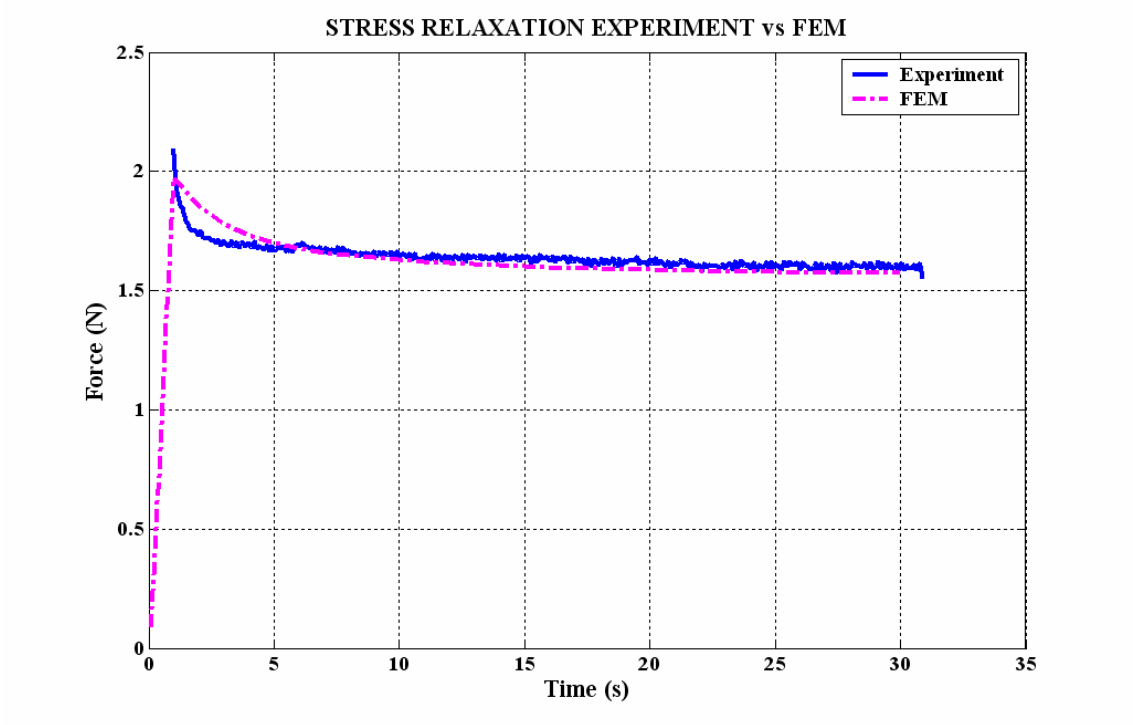

Figure 4.17: Stress Relaxation Experiments and finite element simulations

In order to demonstrate the good match between the experiment and the simulation results, we repeated the compression experiments experimentally and numerically as in Section 4.1.2. CLD data for static compression of 4 mm was obtained and the experimental and model predicted results are compared in Figure 4.18. As it can be seen from the figure, the results are very similar. Inverse Finite Element Solution technique has proven itself to be an accurate and efficient way to determine the viscoelastic and hyperelastic material properties.

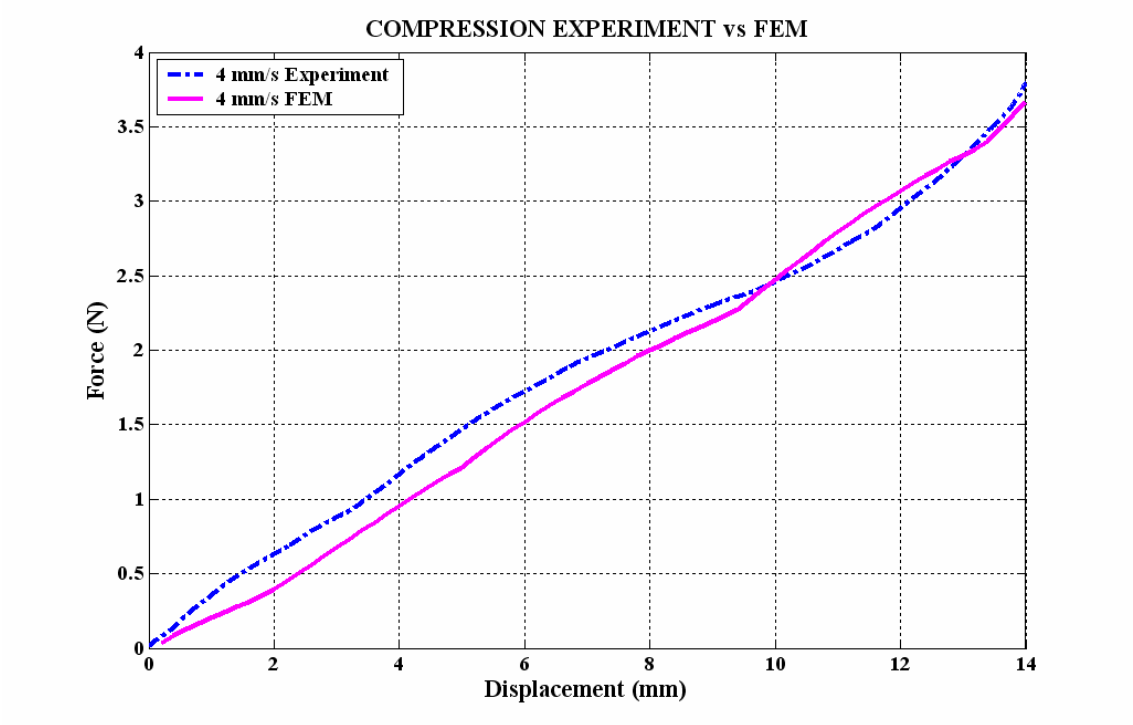

Figure 4.18: Compression experiments and FE simulations with the material properties obtained from inverse FE solution

Chapter 5

LINEAR MODELING OF THE WEATHERSTRIP SEAL

5.1 Introduction

As described in the previous chapter, weatherstrip seal has a nonlinear material behavior. However, such behavior is very difficult to model in modal analysis simulations using commercial finite element codes. One of the reasons for this difficulty is that the theory of small amplitude vibrations in deformed viscoelastic solids is not implemented in many of the commercial finite element codes such as ANSYS. In such a case modal analysis simulations can not be performed using nonlinear material models. The other reason is the extremely high computational cost of simulations performed using the programs in which the theory of small amplitude vibrations in deformed viscoelastic solids is implemented. For these reasons a linear equivalent model of the weatherstrip seal was built using a SDOF system.

Pan et al. [1] proposed an experimental method of evaluation of stiffness and damping characteristics of rubber structures by utilizing the measured frequency response function from impact test. We constructed a single degree of freedom system and used this method to obtain spring-dashpot equivalent of the weatherstrip seal.

5.2 Single Degree of Freedom System

A single degree of freedom system was built in order to determine an equivalent spring damper model for the weatherstrip seal (see Figure 5.1). A mass block and two weatherstrip seals are used to construct the testing system. Force was applied in the center of the block and response of the system was measured by two accelerometers attached on each side of the mass block. This arrangement cancels or minimizes the effect of rocking motion modes on the measured frequency response function. Soft rubber tip was attached to the impact hammer in order to generate low frequency force components and the data was averaged in each test to minimize the effect of random noise.

The equation of motion for this system is represented as [23]:

$$[-m\omega^2+k(\omega)(1+j\eta(\omega))]\,x(\omega)=F(\omega) \tag{5.1}$$

Where ω is the frequency, F is the applied force, k is the frequency dependent stiffness and η is the structural damping coefficient. From Equation (5.1), the complex receptance function can be written as [1]:

$$R=\frac{x}{F}=\frac{1}{k[(1-r^2)+\eta j)]} \tag{5.2}$$

Where $r=\omega/\omega_n$ is the frequency ratio and $\omega_n=\sqrt{\frac{k}{m}}$ is the natural frequency of the SDOF system. The real and imaginary parts of the complex receptance are deducted as [1]:

$$\mathrm{Re}(R) = \frac{1 - r^2}{k[(1-r^2)^2 + \eta^2)} \tag{5.3}$$

$$\mathrm{Im}(R) = \frac{-\eta}{k[(1-r^2)^2 + \eta^2)} \tag{5.4}$$

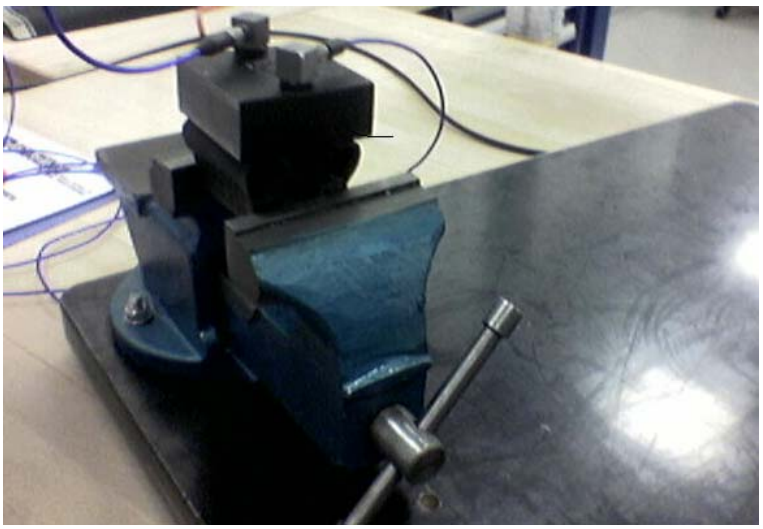

Figure 5.1: Experimental setup to determine equivalent stiffness and damping

And following equations for the frequency dependent stiffness and structural damping are obtained from the Equations. (5.3)-(5.4):

$$\eta = -\frac{\mathrm{Im}(R)}{\mathrm{Re}(R)}(1-r^2) \tag{5.5}$$

$$k = -\frac{\mathrm{Re}(R)}{|R|^2\,(1-r^2)} \tag{5.6}$$

Where |R| is the magnitude of the complex receptance. Accelerance frequency response function $A(\omega) = \frac{\ddot{x}}{F}$ is measured and modified to receptance. Therefore Re(R), Im(R), |R| and ω_n are obtained directly from the measurements. Figure 5.2 and 5.3 illustrate frequency dependent stiffness and damping values.

Stiffness and damping reaches to a peak having their maximum value at resonance which is at 12.71 Hz. Between 14-22 Hz, the stiffness deviates significantly and beyond 22 Hz, it changes between 2000-3000 Hz. Structural damping deviates much more. This may be due to the fact that the shape of the weatherstrip seals changes after every impact and the system exhibits nonlinear behavior with the changing force which results in unreliable data for structural damping. Also, experimental errors may result in variations while calculating stiffness, especially damping.

A constant structural damping coefficient is also calculated at resonant frequency from the half power bandwidth method and equivalent stiffness is calculated from the natural frequency using the formulas below:

$$\eta = \frac{\Delta\omega}{\omega_n} \tag{5.7}$$

$$\omega_n = \sqrt{\frac{k}{m}} \tag{5.8}$$

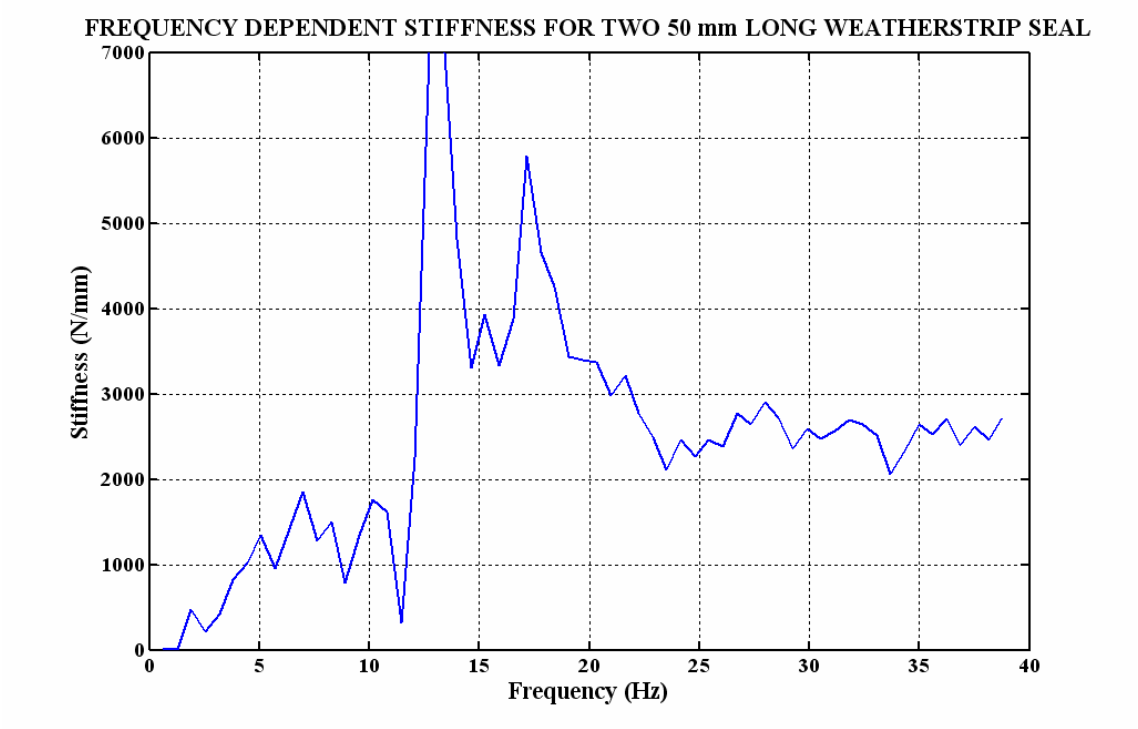

Figure 5.2: Frequency dependent stiffness

From the experiments natural frequency ω_n is measured as 12.71 Hz and constant stiffness and damping are calculated from the Equations 5.7 and 5.8 as k=2642.5 N/m and η=0.109 for the SDOF system with a block and two 50 mm long weatherstrip seals.

After the FRF data was measured, it was transferred to a modal analysis software, ME'Scope VES. ME'Scope VES calculates the viscous damping ratio ξ, by curve fitting the FRF data to a parametric form. Following formulas relating structural damping coefficient η to viscous damping coefficient c and viscous damping ratio ξ to damping coefficient c are given below:

$$c = 2m\omega_n\xi \tag{5.9}$$

$$c_{eq} = (k\eta)/\omega_n \qquad (5.10)$$

Viscous damping coefficient c is calculated by ME'Scope VES as 2.55 and equivalent viscous damping coefficient from the half power bandwidth method is 3.05. Damping ratios from the half power method and ME'Scope VES are not very similar. As explained previously calculated damping ratio is thought to be unreliable due to geometrical and material nonlinearities.

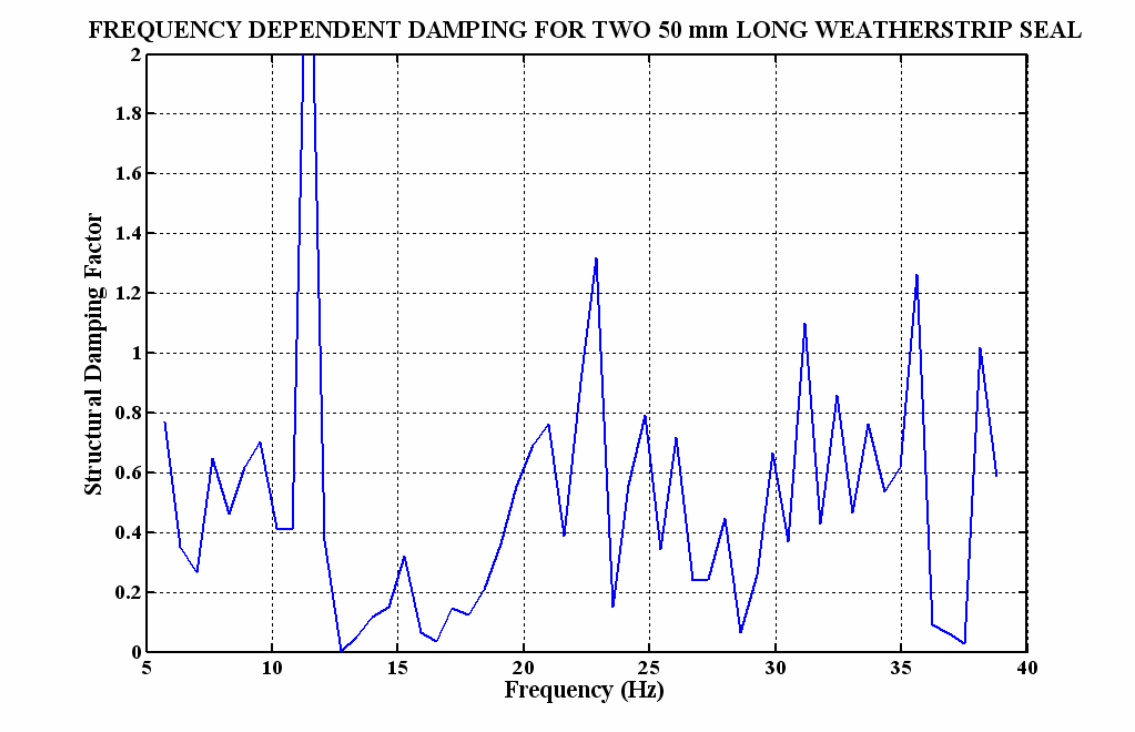

Figure 5.3: Frequency dependent structural damping factor

Chapter 6

MODAL ANALYSIS OF CAR REAR DOOR

As it was discussed in the previous sections, the vehicle door is one of the noise sources contributing to the overall panel vibrations. Boundary conditions and the weatherstrip seals affect the dynamics of the doors considerably. Experimental and Computational Modal Analysis may be used to determine these effects on door dynamics. In this study, two configurations were used to understand the effect of boundary conditions and weatherstrip seals on the vehicle dynamics. The following sections describe the details of the experimental set-ups. Then, computational modal analysis is performed with the spring coefficients found in Chapter 5.

6.1 Experimental Modal Analysis of the Rear Door

6.1.1 Frequency Response Function (FRF) Measurement Techniques

Frequency response functions which relate the input excitation force to response (in the form of acceleration and/or velocity and/or displacement) at various points on the structure are required for the modal analysis of a structure. A typical measurement set-up in a laboratory environment should have three constituent parts. The first part is responsible for generating the excitation force and applying it to the test structure; the second part is to measure and acquire the response data; and the third part provides signal processing

capacity to derive FRF data from the measured force and response data [18]. FRF is the ratio of the response to the excitation force. Table 6.1 illustrates the FRF types according to the measured response.

Table 6.1: FRF types with different response parameters

Response Parameter (R)	FRF (Response/Force)	Inverse (Force/Response)
Displacement	Receptance Admittance	Dynamic Stiffness
Velocity	Mobility	Mechanical Impedance
Acceleration	Inertance Accelerance	Apparent Mass

The first part of the measurement set-up is an excitation mechanism that applies a force of sufficient amplitude and frequency contents to the structure. There are different types of excitation equipment that are able to excite a structure. The two most common ones are shaker and impact hammer. In this study, both impact hammer and electro magnetic shaker were used as the excitation source. In the shaker tests, the velocity response was measured with a laser doppler vibrometer and the input was measured using a force transducer between the shaker and the structure. However, in the impact hammer experiments, the response was measured using accelerometers and the input was measured using the force transducer at the hammer tip.

An impact hammer is a device that produces an excitation force pulse to the test structure. It consists of hammer tip, force transducer, balancing mass and handle (Figure 6.1). The hammer tip can be changed to alter the hardness. Typical materials for the tip are rubber, plastic and steel. The hardness of the tip together with that of the structure surface to be tested is directly related to the frequency range of the input pulse force. For a hard tip striking on a hard surface, we can expect the force pulse to distribute energy to a wide range of spectrum. The stiffer the materials, the shorter will be the duration of the pulse and the higher will be the frequency range covered by the impact. A stiffer tip than necessary will result in energy being input to vibrations outside the range of interest at the expense of those inside the range [18].

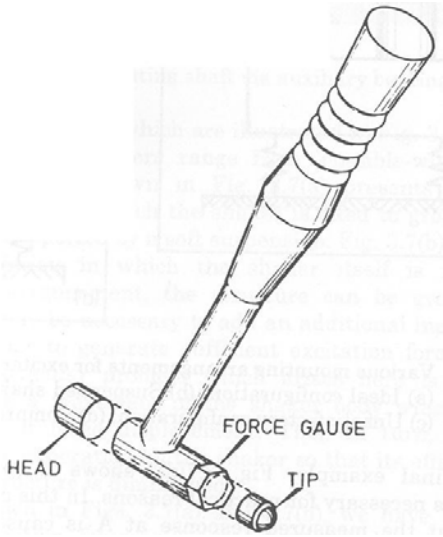

Figure 6.1: Impact hammer and its components [24]

An electromagnetic shaker, also known as an electrodynamic shaker is the most common type of shaker used in modal testing. It consists of a magnet, a moving block and a coil in the magnet. When an electric current from a signal generator passes through the

coil inside the shaker, a force proportional to the current and the magnetic flux density is generated which drives the moving block. An electrodynamic shaker has a wide frequency, amplitude and dynamic range.

An accelerometer is a very common sensor to measure the response of a structure for modal testing. It measures acceleration of a test structure and outputs the signal in the form of voltage. This signal will be transformed by a signal conditioner before it is processed by an analyzer. A most common type of accelerometer is the piezoelectric one as illustrated in Figure 6.2. The accelerometer mass has the potential to change the characteristics of the test structure [18].

Correct location and installation of accelerometers, is important. There are various means of fixing the accelerometers to the surface of the test structure. Threaded stud requires the appropriate modification of the test structure which is not always possible. Magnet attachment, holding by hand and applying thin layer of wax are other alternatives [24]. In our modal analysis experiments, we glued the threaded strud to the test structure.

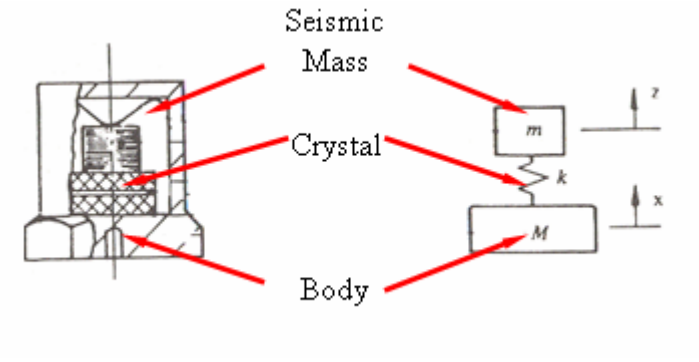

Figure 6.2: Accelerometer and its inner set-up [24]

A laser doppler vibrometer (LDV) is a non contacting vibration measurement device capable of measuring the response in the form of velocity. We used Polytec PDV 100 LDV (Figure 6.3) in our test with superior features compared to accelerometers. The LDV has

the following features: non-contacting velocity measurement in the frequency range 0 to 22 kHz, variable working distance from 0.2 m up to 30 m, analog and digital signal output.

Figure 6.3: PDV 100 Laser Doppler Vibrometer

A force transducer is another type of sensor used in modal testing. Like an accelerometer, a piezoelectric force transducer generates an output charge or voltage that is proportional to the force applied to the transducer (Figure 6.4). Unlike an accelerometer, a force transducer does not have an inertial mass attached to the transducing element. For a shaker test, a force transducer has to be connected between the structure surface and the shaker. For a hammer test, the transducer is located at the hammer tip and is compressed when impact is applied.

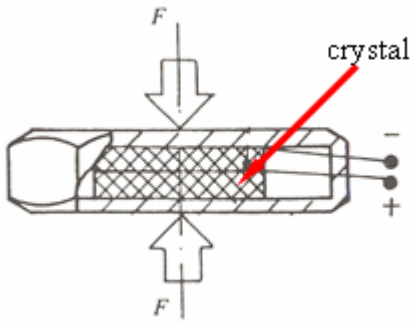

Figure 6.4: Piezoelectric force transducer [18]

6.1.2 Experimental Setup

In order to determine the effect of weatherstrip seal and boundary conditions on the door dynamics, two different configurations were used to perform the modal analysis experiments. In the first configuration, the door was hung from a supporting frame with elastic cords to simulate the free-free boundary conditions. In the second one, doors were mounted to the vehicle body and the whole structure was suspended through air springs. To observe the dynamics of the door on real boundary conditions, half of the vehicle body was used in the second configuration. Air springs with a low natural frequency were selected to satisfy the free-free condition. The two configurations are shown in Figure 6.5.

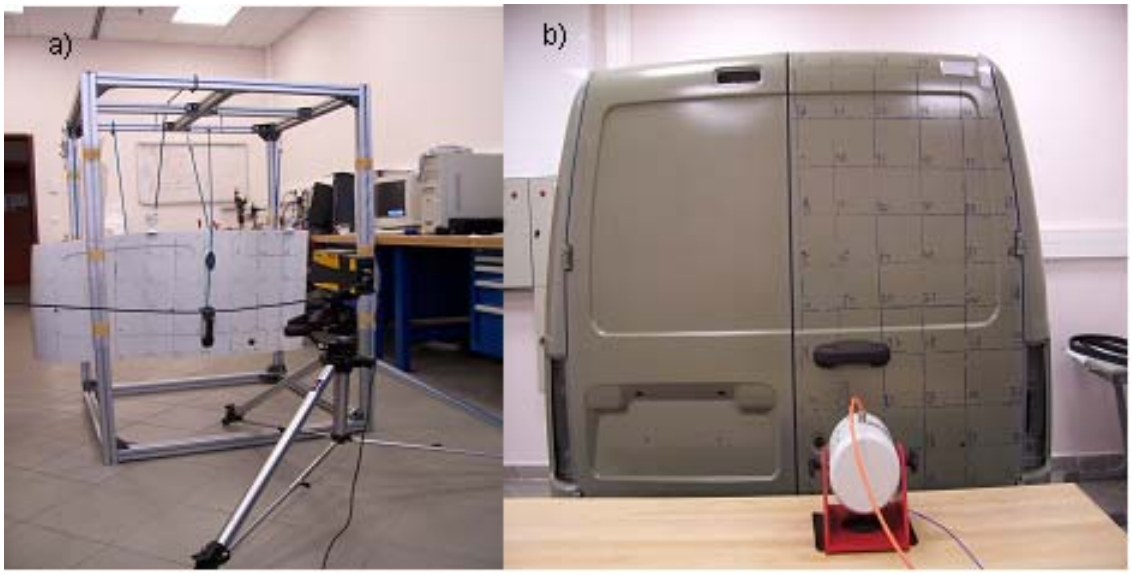

Figure 6.5: The two configurations used for the experimental modal analysis of the door a) Door hung freely b) Door mounted to the vehicle body

Frequency shifts and damping contribution of weatherstrip seals on the door was investigated by performing experiments with and without the seal using the second configuration. The effect of boundary conditions was observed by comparing the experiments in the first and the second configurations without the seal. The experimental set-up included a laser doppler vibrometer (LDV) that was used to pick up signals without contacting the structure. The structure was excited at a wide frequency range by an electrodynamic shaker and the velocity data measured by LDV was collected through the use of a data acquisition system. The transfer functions that relate the excitation input to velocity output were measured at various locations of the structure and then transferred to modal analysis software, ME'Scope VES, to extract the modal parameters. All the experiments are validated by performing an impact hammer test on the structure.

6.1.3 Results of Experimental Modal Analysis of the Door and Discussion

We observed a change in the first and second modes in both configurations. In the free-free boundary condition experiment, the first mode of the door was observed at 37.89 Hz. Then, experimental modal analysis of the same door was performed using the second configuration. The first mode shifted to a frequency of 42.06 Hz in the existence of the weatherstrip seal. Finally weatherstrip seal was removed from all of the contacting surfaces. It was observed that the first mode was altered to 32.93 Hz in the absence of the weatherstrip seal. All of the experiments were repeated using an impact hammer and accelerometers. Similar results were obtained. Figure 6.6 illustrates the first mode shape of the rear door obtained from the experiments with first and second configuration in which the weatherstrip seal was removed. Therefore, the only difference between these two configurations was boundary conditions such as hinge connections and locks.

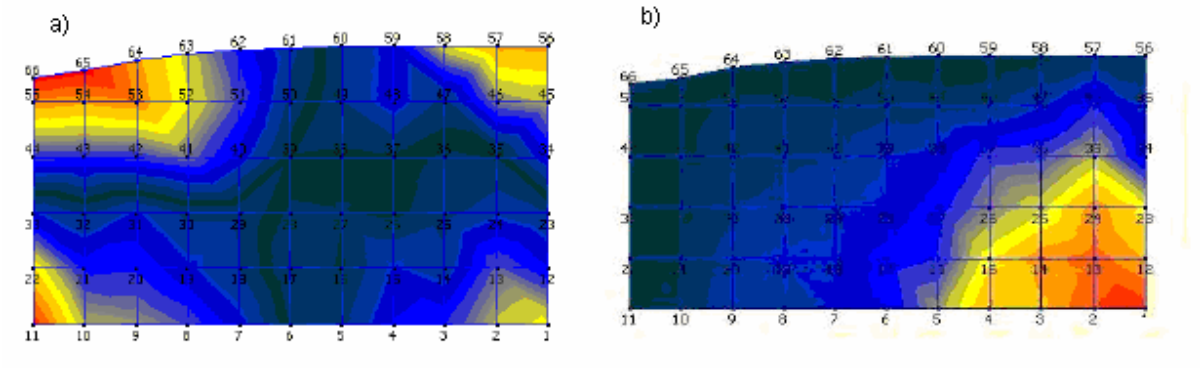

Figure 6.6: Mode shape of the door a) hung freely b) on car without the seal

Boundary conditions changed the first natural frequency from 37.89 to 32.93 Hz. Due to hinge connections around the points 63 and 58 in the above figures; the motion of left and right corners of upper part disappeared in Figure 6.6b. Hence, boundary conditions both alter the natural frequency and the mode shape. The effect of weatherstrip seal in door dynamics can be seen in Figure 6.7. Frequency of the first mode dropped considerably from 42.06 Hz to 32.93 Hz when the seal was removed. However the mode shape was similar. Seal behaves like a spring, hence increased the stiffness radically and affected the dynamics of the door considerably.

Frequency shift of the second mode was less than the first mode where it changed from 64.88 Hz to 61.44 Hz when the seal is removed (see in Figure 6.8). Previous studies indicate that the effect of seal decreases in higher frequencies [5], [7]. When we compare the results for the cases with and without the seal, it is observed that the small amplitude vibrations in right part of the door damped out when the seal was in place.

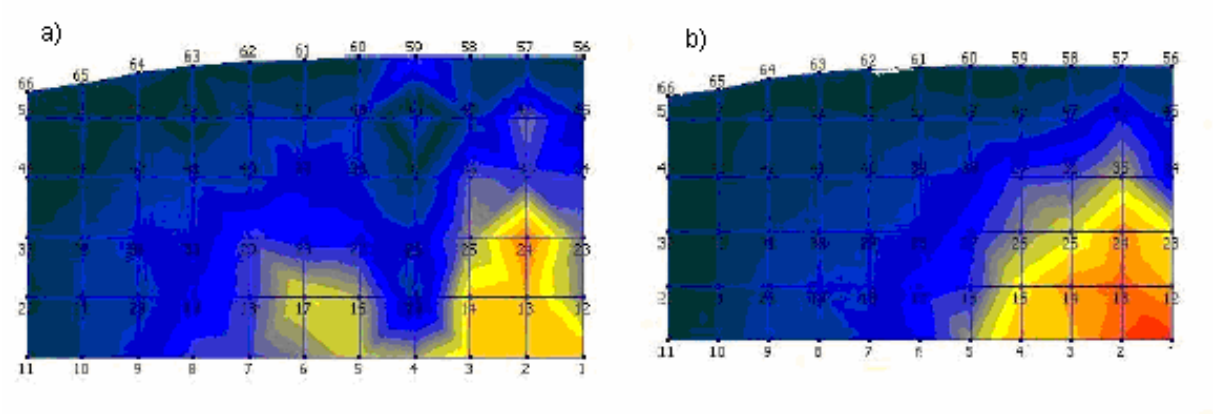

Figure 6.7: First Mode shape of the door on the car with real boundary conditions
a) with the seal at 42.06 Hz b) without the seal at 32.93 Hz

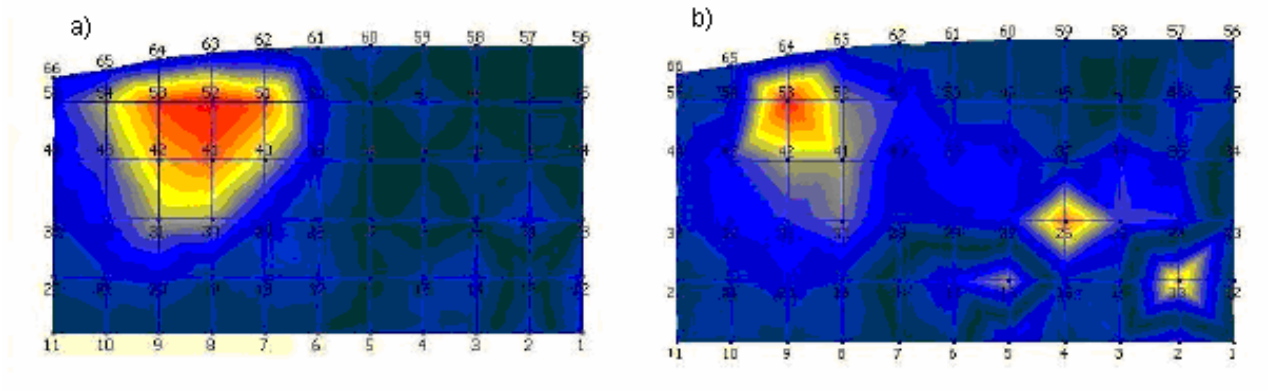

Figure 6.8: Second Mode shape of the door on the car
a) with the seal at 64.88 Hz. b) without the seal at 61.44 Hz

Table 6.2 illustrates the experimental modal analysis result with different boundary conditions and configurations.

Table 6.2: The experimental modal analysis results

	Free-Free Condition	**With The Seal**	**Without the seal**
First Mode	37.89 Hz	42.06 Hz	32.93 Hz
Second Mode	75 Hz	64.88 Hz	61.44 Hz

6.2 Finite Element Simulation Results and Comparison

Finite element simulations of the door were performed with the spring coefficients found in Chapter 5 instead of the weatherstrip seal. FE model is shown below:

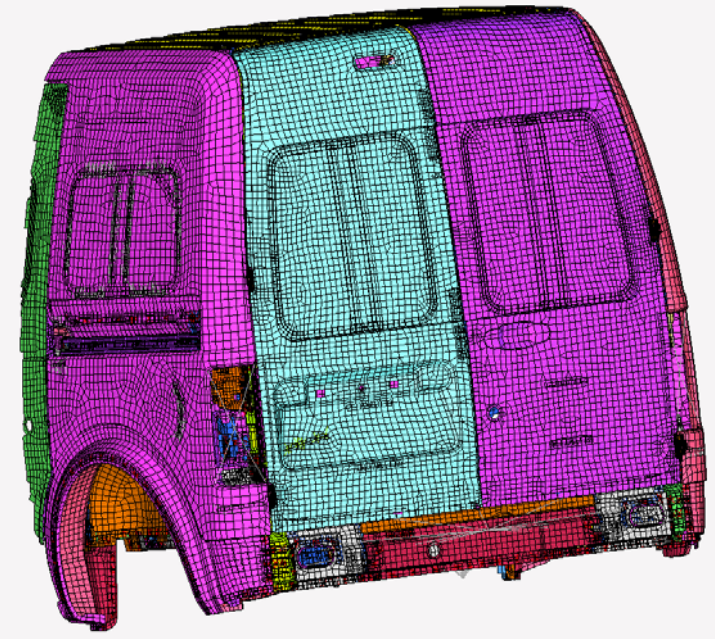

Figure 6.9: Finite Element Model of the half car body

Equivalent spring coefficients are used instead of the weatherstrip seal. Stiffness values of 2000, 2642.5 and 3000 N/m are used for 100 mm long weatherstrip seal in simulations. Simulation results of the first modal frequency are given in the following table.

Table 6.3: Modal frequencies obtained with the specified stiffness value instead of the seal

	k=2000 N/m	k=2642.5 N/m	k=3000 N/m	Experiment
First Modal Frequency	41.449 Hz	41.647 Hz	41.815 Hz	42.06 Hz

Stiffness is calculated from natural frequency is 2642.5 N/m. Stiffness changing with frequency is calculated from the Eqn.18 ranges from 2000 N/m to 3000 N/m.

Around 40 Hz, stiffness is calculated as 3000 N/m which results in the best approximation for the weatherstrip seal. Modal Shapes from the experiments and simulations are shown below in Figure 6.10.

It is observed that stiffness values determined from the SDOF system can be used to model the weatherstrip seal accurately. Using equivalent linear springs instead of the weatherstrip seal decreases the computational cost drastically. Therefore accurate equivalent spring stiffness values for the weatherstrip seal can be obtained practically from the modal analysis of SDOF system with a mass block and weatherstrip seals beneath.

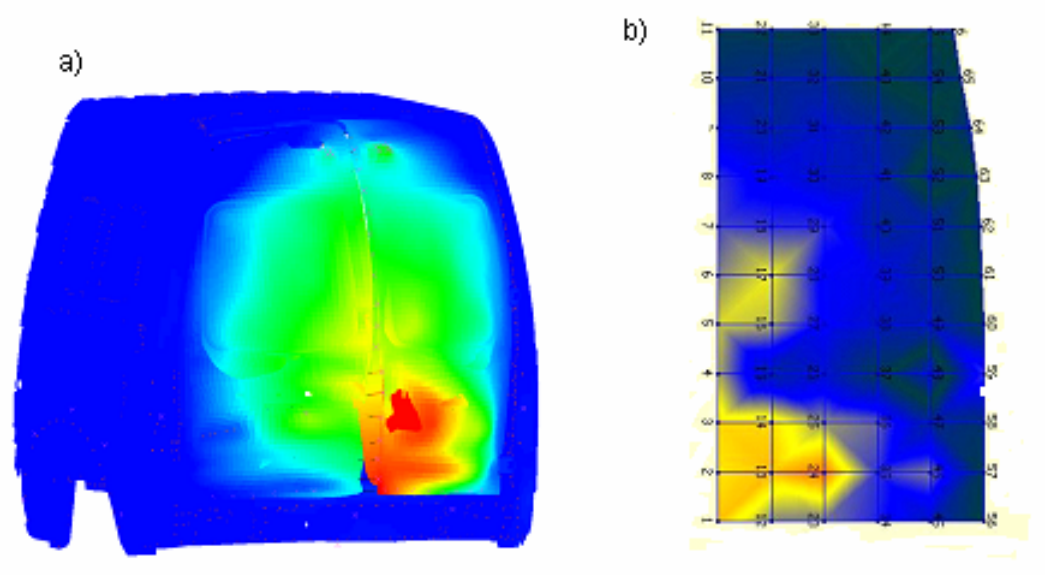

Figure 6.10: Mode shapes of the simulation (a) and experiment results (b)

Chapter 7

CONCLUSIONS AND FUTURE WORK

7.1 Conclusions

In this study, FEM was used to determine the CLD behavior of automobile weatherstrip seals with different hyperelastic models and the model predictions were compared with the experimental results. Arruda-Boyce model was found to be the most suitable strain energy function for modeling the weatherstrip seals. The “Mullins effect” and “friction coefficient effect” were also investigated and they were found to be insignificant for this type of application.

The “Inverse Finite Element” approach was used to determine the hyperelastic and viscoelastic material properties of the weatherstrip seal. This approach was found to be practical and accurate to determine the nonlinear material properties of the weatherstrip seal.

The nonlinear modeling of the weatherstrip seal was found to be very time consuming for the overall vehicle dynamics simulations. Therefore, an equivalent spring and dashpot system for the weatherstrip seal was studied to simplify the weatherstrip seal in the FEM. A SDOF system was built to model the weatherstrip seal as a spring and dashpot system. Equivalent stiffness and damping coefficients for the weatherstrip seal were determined from the experimental modal analysis of this system.

Finally, modal analysis of the rear door was performed using the two different configurations to determine the effect of the seal and boundary conditions on the vehicle dynamics. Boundary conditions both altered the natural frequency and the mode shape of the door. In addition, it was observed that the weatherstrip seal had a significant contribution in the first mode than the second mode. It increased the stiffness and generated a shift in the frequency of the door considerably. Finally, equivalent stiffness coefficients calculated from the SDOF set-up were used in the FE analysis as spring elements instead of the weatherstrip seal. The finite element and experimental modal analysis results were compared to verify the equivalent spring models used for the weatherstrip seal. As a result the SDOF setup was observed to be accurate and practical to determine equivalent stiffness for the weatherstrip seal simplifying the finite element model and decreasing the computational cost.

7.2 Future Work

As a future work, viscoelastic & hyperelastic models can be utilized to perform harmonic analysis with MSC MARC or NASTRAN since ANSYS does not have this feature. The verification of the finite element model of the vehicle utilizing the experimental modal analysis results is another study that could be done in future. The effect of weatherstrip on door closing efforts, the effect of temperature on mechanics of the weatherstrip seal and analysis of door weatherstrip seal systems for aspiration may be further topics for investigation.

BIBLIOGRAPHY

[1] T. R. Lin, N.H. Farag, J. Pan, Evaluation of frequency dependent rubber mount stiffness and damping by impact test, Applied Acoustics, 66 (2005), 829-844.

[2] N.M Vriend, A.P. Kren, Determination of the viscoelastic properties of elastomeric materials by the dynamic indentation method, Polymer Testing, 23 (2004), 369-375.

[3] A. Fenander, Frequency dependent stiffness and damping of railpads, Proc Instn Mech Engrs, 211 Part F (1997), 51-62.

[4] D.A. Wagner, N.M. Kenneth, Y. Gur, M.R. Koka, Nonlinear analysis of automotive door weatherstrip seals, Finite Elements in Analysis and Design, 23 (1997), 33-50.

[5] A Stenti, D. Moens, W. Desmet, Dynamic modeling of car door weather seals: A first outline, ISMA 2004 International Conference on Noise & Vibration Engineering, Leuven, Belgium (2004), 1249-1260.

[6] Z.H. Lu, L.R. Wang, I. Hagiwara, Finite Element simulation of the static characteristics of a vehicle rubber mount, Proc Instn Mech Engrs, 216(D) (2002), 965-973.

[7] A. Tuncer, Effect of Weatherstrip seal stiffness on vehicle vibration and acoustics, M.Sc. Thesis, Bogazici University, 2005.

[8] L. Valente , L. Molnar, Vergleich des Neohooke'schen und Mooney-Rivlin'schen Material models in der FEM Brechnung, Periodica Polytechnica Ser. Mech. Eng.(45) (2001), 95-101.

[9] Y. Gur, K.N. Morman and N. Singh 971902 SAE. Analysis of Door and Glass Run Seal Systems for Aspiration, (1997) 255-270.

[10] T.C. Lim Automotive panel noise contribution modeling based on finite element and measured structural-acoustic spectra, Applied Acoustics (60)(2000), 505-519.

[11] S. Marburg, H.J. Hardtke, A general concept for design modification of shell meshes in structural-acoustic optimization Part II: Application to a floor panel in sedan interior noise problems, Finite Element in Analysis and Design (38) (2002), 737-754.

[12] S.H. Kim, J.M. Lee, M.H.Sung, Structural-Acoustic coupling analysis and application to noise reduction in a vehicle passenger compartment, Journal of Sound and Vibration (225) (1999), 989-999.

[13] S. Marburg, H.J. Beer, J. Gier, H.J. Hardtke, R. Rennert, F. Perret, Experimental verification of structural acoustic modeling and design optimization, Journal of Sound and Vibration (252) (2002), 591-615.

[14] ANSYS, Inc. Basic Structural Nonlinearities. Training Manual for Release 5.6 (2000).

[15] P. Macioce, Viscoelastic Damping.
http://www.roushind.com/news_downloads/white_papers/SV_Damping101.pdf

[16] W. N. Findley, J.S. Lai, K. Onaran, Creep and Relaxation of Nonlinear Viscoelastic Materials, Dover, New York, (1976).

[17] S. Shaw, J. R. Whiteman, Robust Adaptive Finite Element Schemes for Viscoelastic Solid Deformation: An Investigative Study", Final report for the US Army's European Research Office Seed Project, (1999).

[18] J. He, Z.F. Fu, Modal Analysis, Butterworth-Heinemann, (2001).

[19] K. Miller, Testing Elastomers for hyperelastic material models in finite element analysis, Axel Products, (2000).
http://www.axelproducts.com/downloads/TestingForHyperelastic.pdf

[20] E. Samur, Minimally Invasive Characterization and Real-Time Simulation of Viscoelastic Soft Tissue Behavior, M.Sc. thesis, Koc University, (2005).

[21] J.E. Mark., B. Erman, F.R. Eirich, The Science and Technology of Rubber, Elsevier Academic Press, (2005).

[22] M. Sjoberg, L. Kari, Testing of nonlinear interaction effects of sinusoidal and noise excitation on rubber isolator stiffness, Polymer Testing, 22 (2003), 343-351.

[23] A.D. Nashif, D. Jones, J.P. Henderson, Vibration damping. Wiley, (1985).

[24] D.J.Ewins, Modal Testing: theory, practice and application second edition, Research Studies Press , (2000).

PUBLICATIONS

1. Emre Dikmen, Ipek Basdogan, **"Experimental and Numerical Study for determining the mechanical properties of automobile weatherstrip seals",** submitted to 8th Biennial ASME Conference on Engineering Systems Design and Analysis, ESDA 2006, Torino, Italy.

2. Emre Dikmen, Ipek Basdogan, **"A study on modal characteristics of a commercial vehicle rear door**" , submitted to International Conference on Noise and Vibration Engineering, ISMA 2006, Leuven, Belgium.

3. Emre Dikmen, Ipek Basdogan, **"Nonlinear and Linear Modeling of Weatherstrip Seal and Investigation of its Effects in Vehicle Vibrations",** journal paper to be submitted.

VITA

Emre Dikmen was born in Ankara, Turkey on September 4, 1981. He received his B.S. degree from Mechanical Engineering Department of Middle East Technical University, Ankara, Turkey in 2004 with honors degree. From September 2004 to August 2006, he worked as a teaching and research assistant in Koç University, Istanbul, Turkey. He presented a conference paper at ESDA 2006, 8th Biennial ASME Conference on Engineering System Design and Analysis, July, 2006, Turin, Italy, and a poster paper at ISMA 2006, International Conference on Noise & Vibration Engineering, September, 2006, Leuven, Italy. He has currently one journal paper submission. He plans to further his studies for PhD.